Running head: Spatiotemporal mapping of legume root exudation

***Address correspondence for this author:**
Philip S. Poole
Department of Plant Sciences, University of Oxford
South Parks Road, OX1 3RB Oxford, United Kingdom
Telephone: +44 - (0)1865 - 275023
E-mail: philip.poole@plants.ac.ox.uk

Research area: Breakthrough technologies

Title: Bacterial biosensors for in vivo spatiotemporal mapping of root secretion

Francesco Pini[a], Alison K. East[a,b], Corinne Appia-Ayme[b], Jakub Tomek[c], Ramakrishnan Karunakaran[b], Marcela Mendoza-Suárez[a,b], Anne Edwards[b], Jason J. Terpolilli[b], Joshua Roworth[a], J. Allan Downie[b] and Philip S. Poole[a,b*]

[a] Department of Plant Sciences, University of Oxford, South Parks Road, Oxford OX1 3RB, UK

[b] Department of Molecular Microbiology, John Innes Centre, Norwich Research Park, Norwich NR4 7UH, UK

[c] Department of Physiology, Anatomy and Genetics, University of Oxford, Sherrington Road, Oxford OX1 3PT, UK

One sentence summary:

Development of a suite of rhizobial *lux* reporters to map *in vivo* root exudation, spatially and temporally.

Author Contributions

Conceived and designed the experiments: FP, AKE, and PSP. Performed the experiments: FP, RK, MMS, CAA, AKE, JJT, JR, and AE. Analyzed the data: FP, AKE, and PSP. Software development: JT. Wrote the paper: FP, AKE, JAD, and PSP.

Footnotes:

Financial source: This work was funded by the Biotechnology and Biological Sciences Research Council [grant numbers BB/K001868/1, BB/K001868/2] and a BBSRC Institute Strategic Programme Grant (BIO) at the John Innes Centre.

Address correspondence to philip.poole@plants.ac.ox.uk

The author responsible for distribution of materials integral to the findings presented in this article in accordance with policy described in the Instructions for Authors (www.plantphysiol.org) is:

Philip S. Poole (philip.poole@plants.ac.ox.uk)

Manuscript information:

Word and character count: 219 words in abstract, and 10,069 words in text, comprising Introduction and References

Abstract

Plants engineer the rhizosphere to their advantage by secreting various nutrients and secondary metabolites. Coupling transcriptomic and metabolomic analysis of the *Pisum sativum* rhizosphere, a suite of bioreporters has been developed in *Rhizobium leguminosarum* bv. *viciae* 3841, and these detect metabolites secreted by roots in space and time. Fourteen bacterial *lux*-fusion bioreporters, specific for sugars, polyols, amino acids, organic acids or flavonoids, have been validated *in vitro* and *in vivo*. Using different bacterial mutants (*nodC, nifH*), the process of colonization and symbiosis has been analyzed, revealing compounds important in the different steps of the rhizobial-legume association.

Dicarboxylates and sucrose are the main carbon sources within the nodules; in ineffective (*nifH)* nodules, particularly low levels of sucrose were observed suggesting that plant sanctions affect carbon supply to nodules. In contrast, high *myo*-inositol levels were observed prior to nodule formation and also in *nifH* senescent nodules. Amino-acid biosensors showed different patterns: a GABA biosensor was active only inside nodules, whereas the phenylalanine bioreporter showed a high signal also in the rhizosphere. The bioreporters were further validated in vetch, producing similar results. In addition, vetch exhibited a local increase of *nod*-gene inducing flavonoids at sites where nodules subsequently developed. These bioreporters will be particularly helpful to understand the dynamics of root exudation and the role of different molecules secreted into the rhizosphere.

Additional keywords: Biosensor, Rhizosphere, Root secretion, Legume nodulation, *Pisum, Vicia,* Exudate

Introduction

Due to root secretion, the narrow zone surrounding roots known as the rhizosphere, is a nutrient-rich region where plants encounter a diversity of microbes, fungi, invertebrates and the roots of other plants (Turner et al., 2013a). The constant improvement of sequencing techniques has rapidly increased acquisition of knowledge about rhizosphere communities (Turner et al., 2013b). It is now evident that there is a two-way dialogue, with plants actively shaping their rhizosphere community; this in turn, profoundly alters plant growth e.g. by improving plant nutrient uptake (Philippot et al., 2013). Secretion patterns from roots differ between plants (Biedrzycki and Bais, 2009) and despite much research on the role of chemical signals in mediating belowground interactions (Huang et al., 2014), many factors have not yet been identified (Badri et al., 2009). In addition, spatial and temporal variations in root secretions have never been clearly elucidated. Plant roots secrete large amounts of different compounds into the soil and about 20% of photosynthate is released through the roots (Kaiser et al., 2015). As a consequence of this, compared to bulk soil, the rhizosphere is a rich source of compounds sustaining bacterial growth. This results in the attraction to the rhizosphere of many different microorganisms, amongst them both pathogens and plant growth-promoting bacteria (Huang et al., 2014). Different techniques have been used to study this complex environment; e.g. proteomics, metabolomics and transcriptomics, (reviewed by: Sørensen et al., 2009; Oburger and Schmidt, 2016), but the results obtained with many of these different methodologies is that they give only a single 'snapshot' as it has not been possible to follow the same plant during the course of its development. Current 2D and 3D non-invasive imaging techniques to examine the physical architecture of the plant roots using radiation-based techniques of X-ray microfocus-computed tomography or synchrotron tomography have been described (Mooney et al., 2011). These techniques are powerful at revealing root architecture and development but do not yield information about chemical secretion by roots.

In response to plant secretions, bacteria modify expression of specific genes based on the molecules present in the rhizosphere (Ramachandran et al., 2011). Linking this with a method to monitor gene expression, we have used bacteria as biosensors to detect where and when specific molecules are secreted by plant roots. Bioluminescence is non-invasive and allows measurement of *in situ* differences in the

secretion of specific compounds in a semi-quantitative way. Lux biosensors have already been successfully used (Darwent et al., 2003), but lack of a simple system for image acquisition and complex experimental settings have so far limited routine use. Improvement of the technologies available and an increased knowledge of the bacterial transcriptomic response to roots, now gives us the chance to develop a suite of biosensors. These biosensors have been constructed using *Rhizobium leguminosarum* biovar *viciae*. Rhizobia are alpha-proteobacteria, ubiquitous within soil and able to establish nitrogen-fixing symbioses with specific legumes. Perception of environmental signals plays a pivotal role in association between plants and bacteria (Pini et al., 2011) and *R. leguminosarum* biovar *viciae* modifies its transcriptomic profile in different rhizospheres (Ramachandran et al., 2011). Moreover, the association of *R. leguminosarum* biovar *viciae* with peas has been studied in depth (Oldroyd et al., 2011; Terpolilli et al., 2012; Udvardi and Poole, 2013), making *R. leguminosarum* biovar *viciae* one of the best candidates for biosensor development to investigate the rhizosphere. Pea and vetch plants have been used allowing us to monitor both the rhizosphere and the process of nodulation. Applications of this methodology will be multiple and are not restricted to leguminous plants; e.g. screening plant mutant libraries for those altered in secretion from roots or observing different exudations during seed germination.

158

RESULTS

Solute Specificity of Biosensors

To spatially and temporally investigate secretion in the rhizosphere, we need biosensors able to detect compounds exuded into this environment. The idea that effective biosensors could be constructed using the control elements for expression of specific bacterial genes, often encoding components of solute transporters or enzymes with precise substrate recognition, has been previously described (Tecon and van der Meer, 2006; Yagi, 2007; Sørensen et al., 2009). Induction of expression of genes encoding transporters in the presence of their transported solute led to the identification of the substrates of many ATP-binding cassette (ABC) and tripartite ATP-independent periplasmic (TRAP) transporter systems of *Sinorhizobium meliloti* (Mauchline et al., 2006). Building on these data, Ramachandran *et al*. (Ramachandran et al., 2011) determined which genes of *R. leguminosarum* biovar *viciae* strain 3841 (Rlv3841) are differentially expressed in the rhizospheres of pea, alfalfa and sugar beet, leading to identification of metabolites inducing expression of genes encoding both transport systems and metabolic enzymes. As many of these genes were induced in the rhizosphere in response to specific solutes, we sought to use their expression profiles to develop a suite of biosensors. These biosensors can be grouped by classification of inducer: i) sugars and polyols, ii) organic acids, iii) amino acids and iv) flavonoids (Table I). How each biosensor was selected is described below.

Eleven genes whose expression was induced in the rhizosphere during plant colonization by Rlv3841 of the pea rhizosphere (Ramachandran et al., 2011) were selected for biosensor development (Table I). These include seven solute-specific transport systems (which may transport plant-derived compounds, or those from any source e.g. fungi, other bacteria, within the rhizosphere), and four enzymes from metabolic pathways that are up-regulated during rhizosphere colonization (Table I). To increase the suite of biosensors, an additional two genes were included on the basis of microarray data that show differential expression in response to pea root exudate (Table I) (Ramachandran et al. 2011). The fourteenth biosensor is based on a salicylic acid-inducible export system for salicylic acid (Tett et al., 2014), which is known to be an important signaling molecule in plant defense. Whilst an inducer of gene expression was already known for many of these, the only previous characterization of pRL90085, RL4218, and pRL120556 was that their expression

192 was induced either in the rhizosphere or by pea-root exudate (Table II).
193
194 To develop the *lux*-based induction biosensors, the promoter regions upstream
195 of the selected genes were used, often including the whole coding sequence of any
196 upstream regulatory gene. Following PCR amplification, each region was cloned into
197 the luminescence vector (pIJ11268, a plasmid stably inherited in rhizobia), in front of
198 the bacterial *luxCDABE* operon (Frederix et al., 2014) (Supplemental Table S1). As
199 these biosensors are plasmid-based it is possible to transfer them into different
200 bacterial backgrounds, e.g. mutant strains of *R. leguminosarum* or other species of
201 bacteria, although their expression in heterologous hosts may be limited by regulatory
202 elements (Galardini et al., 2015).
203 Each of the fourteen *lux* reporters was tested on 26 different sugars and
204 polyols and/or on a set of 18 selected compounds (organic acids, amino acids and
205 plant metabolites) to establish the specificity of induction of *lux* expression from each
206 of the bioreporters (Table I, Supplemental Table S2). Nine of the biosensors were
207 induced by only a single compound tested: i.e. the polyols erythritol (pRL90085) and
208 *myo*-inositol (RL4655; *intA*); the organic acids formate (RL4393; *fdsG*), malonate
209 (RL0992; *matA*), tartrate (RL0996) and salicylic acid (RL1329; *salA* encoding an
210 export system for salicylic acid induced by the presence of this molecule (Tett et al.,
211 2014)); the amino acids phenylalanine (RL1860; *phhA*) and GABA (RL0102; *gabT*);
212 and the flavonoid hesperetin (pRL100185; *nodABC*) (Table I). These solutes are
213 considered to be specific inducers, i.e. the specific luminescence is ≥10-fold the
214 specific luminescence induced by the other solutes tested (apart from bioreporters for
215 erythritol, formate, and GABA which have relatively high expression in the presence
216 of a variety of chemically unrelated substrates (background), but show ≥4-fold the
217 specific luminescence of other solutes). However, this definition of specificity, in no
218 way excludes the possibility that these bioreporters may also react with other
219 compounds similar to the molecules which elicit the primary response, but not tested
220 in this work, e.g. it is known that *nod* genes are induced by a variety of different
221 flavonoids (Maj et al., 2010; Maxwell et al., 1989). Another two sugar biosensors
222 were induced by two closely related compounds tested (Table I): i) by two
223 aldopentoses, xylose or lyxose (RL2720; *rbsC*) or ii) induction by the di-saccharide
224 sucrose was also achieved by the tri-saccharide raffinose (pRL120556), presumably
225 because either the biosensor recognizes the sucrose 1-2 β linkage in the di-/tri-

saccharide or raffinose is metabolized to sucrose. A further two bioreporters were induced by three closely related compounds; i) the C4-dicarboxylic organic acids succinate, malate and aspartate all cause induction of a single biosensor (RL3424; *dctA*) and ii) the polyol mannitol (C6) is the main inducer in biosensor (RL4218) although, a weaker induction is elicited also by its isomer sorbitol, and C5 adonitol (Table I) Sorbitol and adonitol are not considered specific inducers as their specific luminescence is <40% that of mannitol (Table I). One bioreporter was induced by six of the tested sugars and polyols, with the main inducer being the mono-saccharide fructose (RL0489; *frcB*). Induction was also seen with di-saccharides lactulose (4-O-β-D-galactopyranosyl-β-D-fructofuranose) and sucrose (α-D-glucopyranosyl-(1→2)-β-D-fructofuranoside). These sugars all share a common structure containing a molecule of β-D-fructofuranose. Furthermore, this biosensor was induced by the polyols mannitol and sorbitol and the monosaccharide mannose. In this case, it is likely that induction occurs due to the catabolism of these compounds to fructose. The fourteen biosensors were used in the following experiments and are henceforth referred to by the compound that elicits the highest-fold change in *lux* expression (Table I). Provided rhizobial survival is not affected, these biosensors should be able to detect the presence of the compound/s for which they are specific, not only in the rhizosphere, whether they are derived from plants, from other bacteria or another source, but also in many other environments.

To discover the limits of detection for each biosensor, the sensitivity (the minimum concentration which causes induction) of the main inducer was determined using a range of different solute concentrations. The sensitivity ranges from the ability to detect levels of 1 μM for mannitol and hesperetin to 10 mM for formate and malonate (Table I).

Data Extraction from Images using NightCROP

Plants were analyzed using the NightOWL, a molecular imaging system linked to a sensitive charged-coupled device (CCD) camera, which allows measurement of light output from the Lux proteins. Images collected were first analyzed with the IndiGO software but although it was used to obtain data for nodules and vetch plants (output in cps / mm^2), a limitation of this software is that it is unable to do an automatic segmentation of the picture, so NightCROP, a custom MATLAB

script, was developed. The script uses the SeNeCA algorithm (Tomek et al., 2013) to segment roots from the background in the light intensity channel, discarding those segments smaller than 1000 pixels. The information on the position of the roots is then used on the luminescence channel to specifically detect the fluorescence signal coming from the roots (Supplemental Fig. S1).

In vivo Mapping of Bacterial Colonization of Pea Roots

Before using the suite of bioreporters to map the rhizosphere, we examined colonization by *R. leguminosarum* bv *viciae* of pea roots *in planta* using Lux mapping. Rlv3841 containing pIJ11282, expressing Lux constitutively under the control of the *nptII* promoter (Frederix et al., 2014), was used to inoculate pea seedling roots and the luminescent images revealed the location on the root of metabolically active Rlv3841. Lux expression relies on the bacteria having enough energy in the form of ATP to drive this energetically expensive production of light. Pea roots were imaged every 3-4 days until 22 dpi, with nodules becoming visible to the naked eye at 11-15 dpi.

At 4 and 8 dpi, luminescence from Rlv3841 colonization was mainly detected in the elongation zone of the lateral and primary roots (Fig. 1). At 11 dpi, overall luminescence was reduced probably due to energy depletion of the bacteria, (Fig. 1), although a signal was still detectable at a lower level (Supplemental Fig. S2). After 15 dpi, there was an increase of the signal concurrent with nodule development, and luminescence was then stable in nodules until 18 dpi, decreasing at 22 dpi, probably due to a general decline of plant health under these growth conditions. This constitutive Lux fusion is an energy sensor that is very effective at showing initial colonization and the total energy available to the bacteria, but must be used with caution in longer-term imaging, dues to depletion of bacterial energy reserves resulting in loss of signal.

In vivo Mapping of Metabolites on Pea Roots and in Nodules

The composition of pea root exudate was determined by metabolomic analysis of hydroponically-grown plants. Although plants grown in different conditions may differ in the composition of their root exudates, metabolomic analysis of these exudates is able to give important indications on compounds that it may be possible to retrieve from the rhizosphere. With the exception of formate, salicylic acid, and

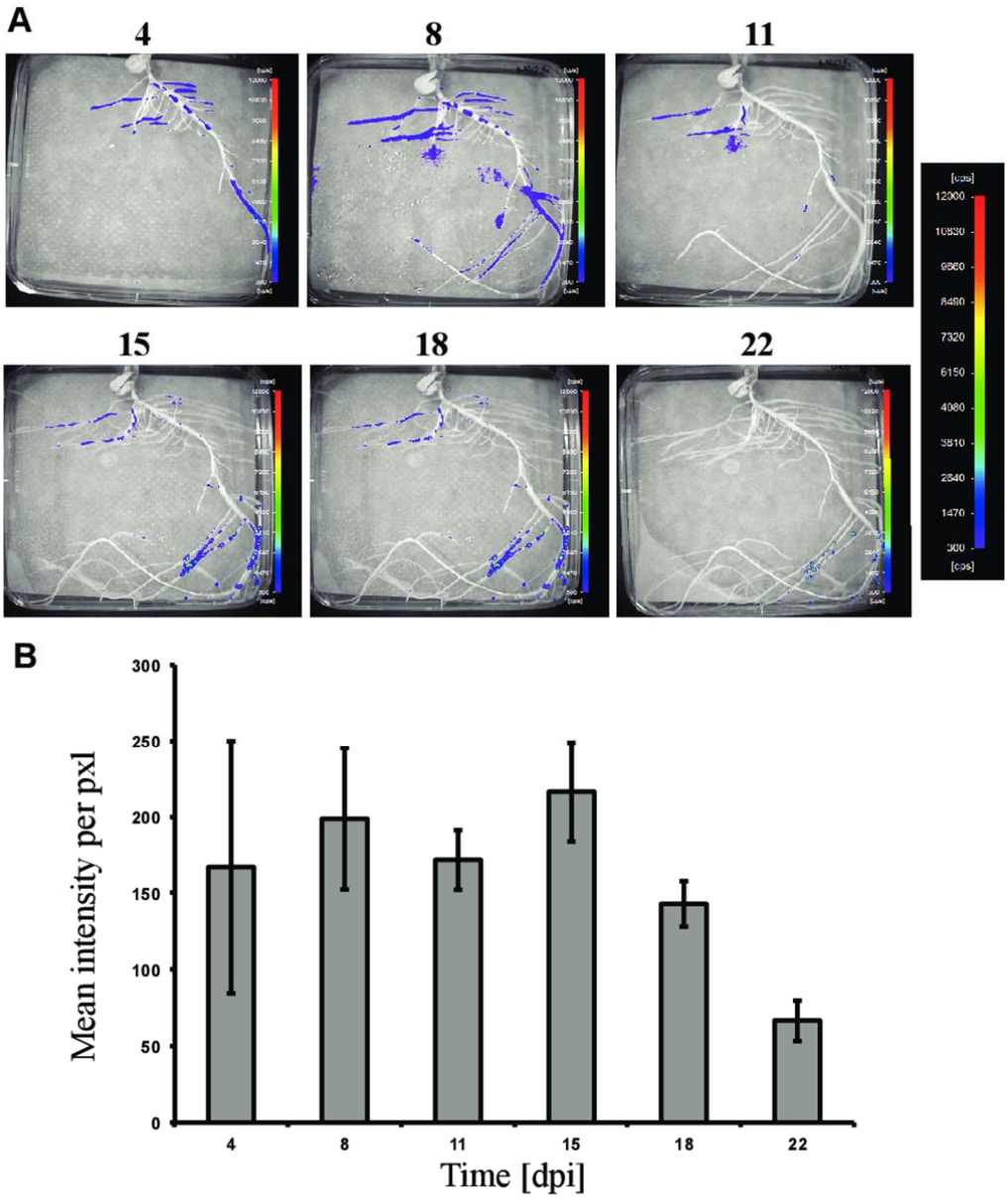

Figure 1. In vivo spatial and temporal mapping images of pea root colonization and nodulation with wild-type Rlv3841 luminescently-labelled with a constitutive neomycin phophotransferase promoter controlling Lux expression in pIJ11282 (Frederix et al., 2014). A, Images were acquired at 4, 8, 11, 15, 18 and 22 dpi, with nodules visible to the naked eye between 11 and 15 dpi. B, Mean luminescence (pxl mm^{-2}) with standard errors shown by bars.

hesperetin, the targets of our biosensors were among the 376 compounds detected in exudate from 23 d-old peas (Table II, Supplemental Table S3). A microarray experiment comparing Rlv3841 grown with and without addition of the same 23 d-old pea root exudates used for the metabolomic analysis was also performed. Results

296 from this are compared to a microarray where *R. leguminosarum* was inoculated into
297 the pea rhizosphere and then harvested 1 dpi from 21 d-old plants (Ramachandran et
298 al., 2011) (Table II). Of the fourteen genes used to develop biosensors, eleven (all
299 except those detecting malonate, salicylic acid and GABA) showed increased (> 3-
300 fold) expression with added pea root exudate and/or in pea rhizosphere-grown cells
301 (Ramachandran et al., 2011) (Table II), however, relative increases in expression in
302 these two experiments do not correlate particularly well. This discrepancy is likely to
303 be due to differences in concentrations of solutes in the two experiments. Indeed,
304 compounds collected from the root (exudate sample) and then diluted into liquid
305 media are very unlikely to be present at the same concentrations as those in the
306 experimental pea rhizosphere. In addition, the exact chemical composition of root
307 exudates will also reflect the two different plant growth conditions. Despite these
308 caveats, expression of approx. 80% of the genes selected to make biosensors are
309 elevated by the conditions of the microarray experiments with added root exudate
310 and/or the pea rhizosphere, which suggests that they will be useful in investigating the
311 pea rhizosphere *in situ*.
312 We analyzed *lux* expression on roots *in vivo* with each of the fourteen biosensors
313 in Rlv3841. To ensure that expression of each biosensor is due to chemicals released
314 from the plant roots, each bioreporter was spotted onto FP agar plates (supplemented
315 with pyruvate and ammonium chloride) and incubated for 7 days (no growing plant
316 present). The images (Supplemental Fig. S3) show no luminescence, thus indicating
317 that the inducing compound is coming from the plant roots. To confirm that the
318 biosensors respond to the same inducers on roots (*in vivo*) as they do *in vitro*, flooding
319 experiments were undertaken. Pea roots at 4 dpi with a specific biosensor were
320 flooded with a solution of a compound shown to induce Lux expression *in vitro*
321 (Table I). Inoculation with the xylose, sucrose or GABA biosensor and flooding with
322 xylose, sucrose or GABA, respectively, induced a Lux signal (Supplemental Fig. S4,
323 A-C). Moreover, flooding the sucrose biosensor-inoculated roots with GABA, and the
324 GABA biosensor-inoculated roots with sucrose showed no increase in Lux expression
325 (Supplemental Fig. S4, D-E).
326 Images representative of those obtained on pea roots for the biosensors for
327 sucrose (a sugar), *myo*-inositol (a polyol), malonate (an organic acid) and
328 phenylalanine (an amino acid) are shown in Fig. 2, A-D. Luminescence images
329 revealed that each of these four biosensors detected target metabolites during the 22

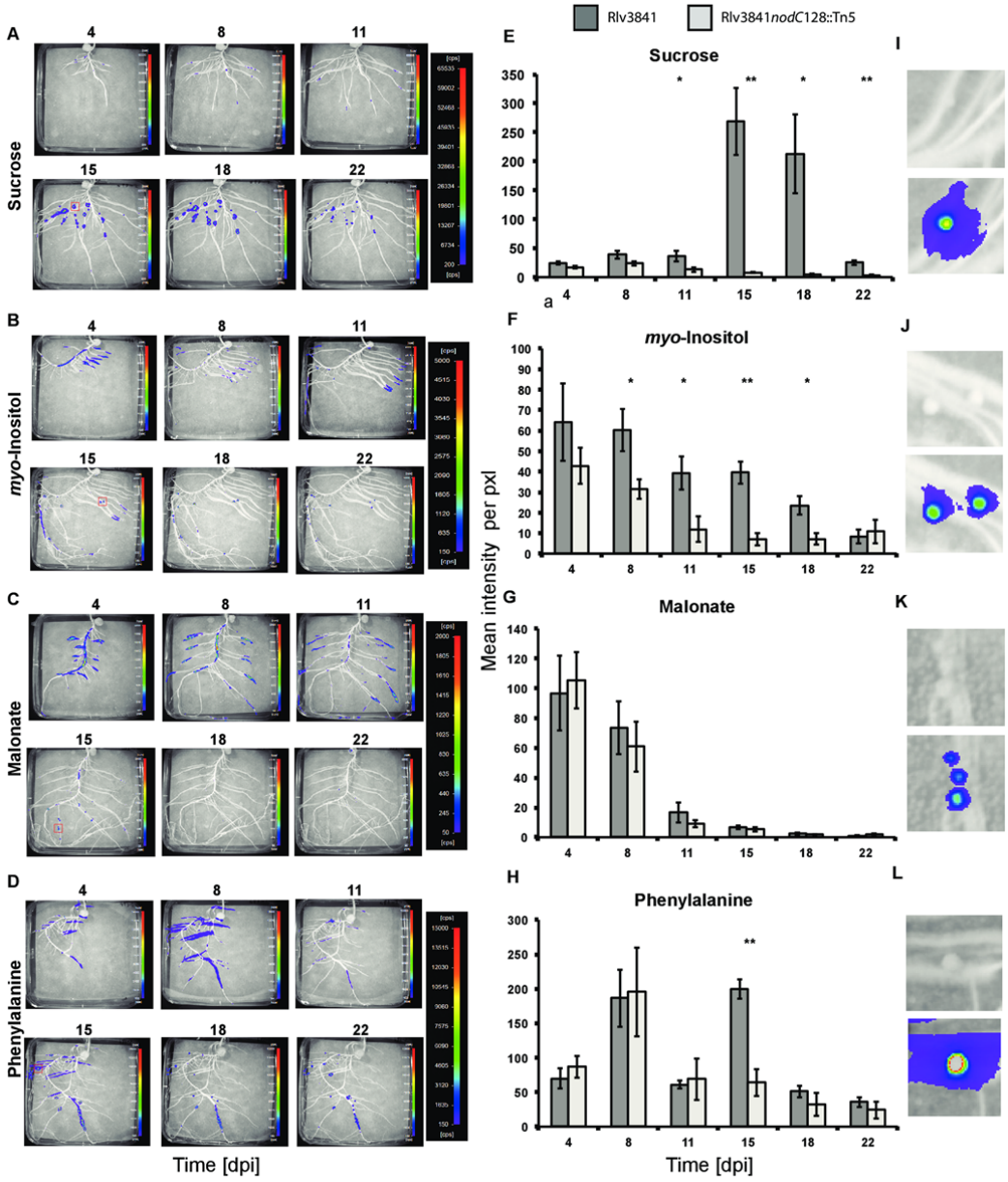

Figure 2. In vivo spatial and temporal mapping images of pea roots with biosensors detecting: sucrose (A) (scale: 200-65,535 cps), myo-inositol (B) (scale: 150-5,000 cps), malonate (C) (scale: 50-2,000 cps), and phenylalanine (D) (scale: 150-15,000 cps). Images were acquired at 4, 8, 11, 15, 18 and 22 dpi, with nodules visible to the naked eye between 11 and 15 dpi. These images are representative of those from biosensors in wild-type Rlv3841 background which nodulates peas. Comparison of mean luminescence intensity per pixel from pea roots inoculated with biosensors in wild-type Rlv3841 background (dark gray) and Rlv3841 nodC128::Tn5 background (light gray). Only wild-type Rlv3841 can form nodules. The biosensors detect: sucrose (E), myo-inositol (F), malonate (G) and phenylalanine (H). Standard errors are shown by bars, stars indicate significant differences between a biosensor in wild-type Rlv3841 and Rlv3841 nodC128::Tn5 backgrounds (t-test, * = $p < 0.05$; ** = $p < 0.01$). Differences between each time point (ANOVA with post hoc Tukey test, $p < 0.05$) are reported in Supplemental Tables S4 and S5. For representative images from Rlv3841 nodC128::Tn5 background see Supplemental Fig. S6. Close-up light-field photograph and luminescence of roots showing nodules at 15 dpi inoculated with biosensors detecting: sucrose (I), myo-inositol (J), malonate (K), and phenylalanine (L).

dpi period, and the results gave not only the location of the detected compound, but also, by following the same plant over time, the changes that occur over the course of an experiment. Bearing in mind that the bacterial cells containing the bioreporter need to be metabolically active to generate a Lux signal, it is possible to get a false negative result, i.e. the inducing compound is present at levels above the minimum sensitivity, but the cells do not have the energy required to produce the signal. The

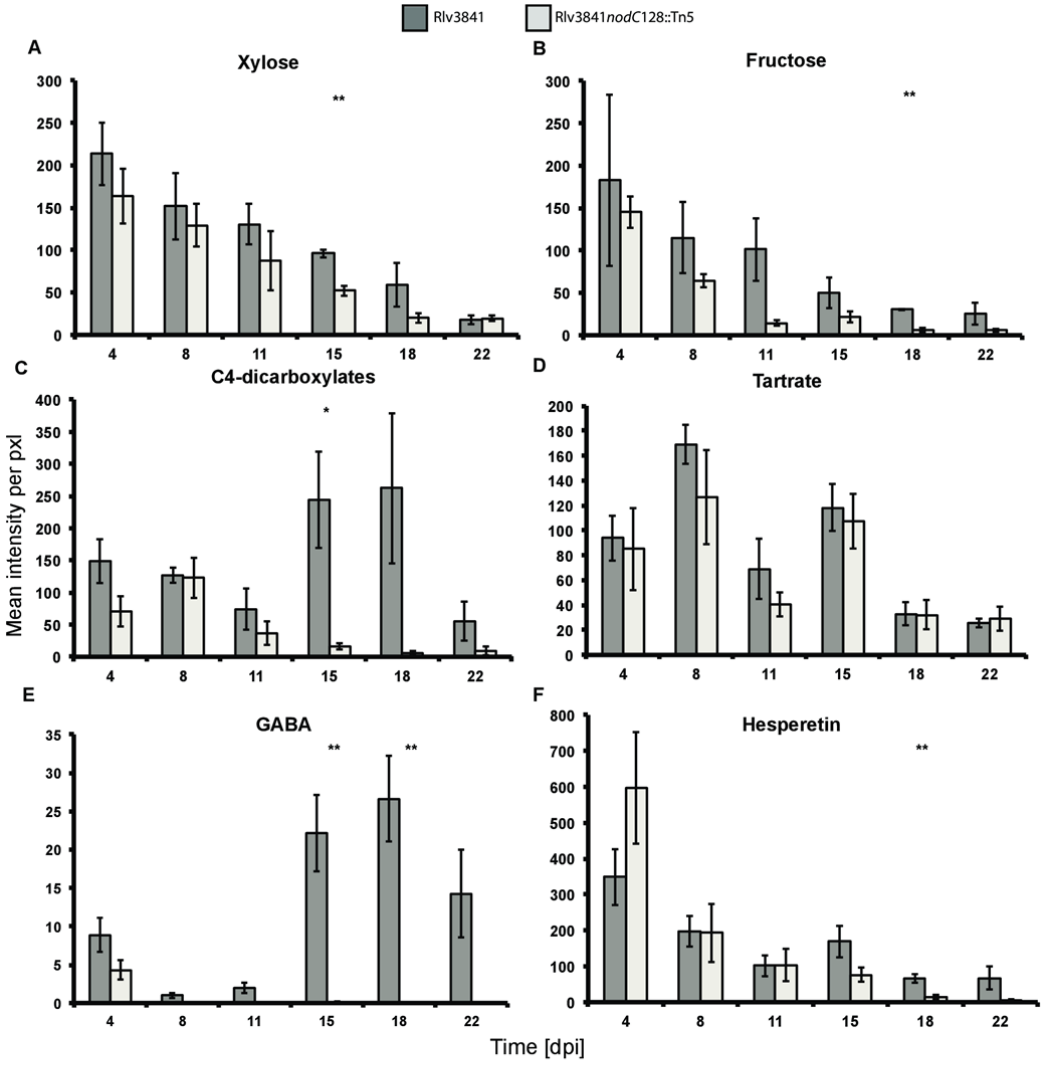

Figure 3. Comparison of mean luminescence intensity per pixel from pea roots inoculated with biosensors in wild-type Rlv3841 (dark gray) or the Rlv3841 nodC128::Tn5 mutant (light gray). Only wild-type Rlv3841 can form nodules. Biosensors detect: xylose (A), fructose (B), C4-dicarboxylates (C) tartrate (D), GABA (E) and hesperetin (F). Standard errors are shown by bars, stars indicate significant differences between a biosensor in wild-type Rlv3841 and Rlv3841 nodC128::Tn5 (t-test, * = $p < 0.05$; ** = $p < 0.01$). Differences between each time point (ANOVA with post hoc Tukey test, $p<0.05$) are reported in Supplemental Tables S4 and S5. For representative images from Rlv3841 and Rlv3841 nodC128::Tn5 background see Supplemental Figs. S6 and S7, respectively.

signal from a constitutive Lux fusion fades over several days because it places a substantial energy drain on cells. However, if Lux is detected, it indicates the inducing compound is present. Analysis of the localization of luminescence in the images (4 or more plants) and the different temporal patterns of metabolite detection during the colonization and nodulation process (Fig. 2, E-H, Fig. 3) revealed that there were similar detection profiles which could be grouped to aid analysis, although the scale and maximum values observed are different for each bio-reporter.

The biosensor for the polyol, *myo*-inositol (able to detect ≥100 µM *myo*-inositol, Table I), was induced in the rhizosphere, mostly on the primary root and near the tips of lateral roots (Fig. 2, B and F), with a steady decrease in expression over time.

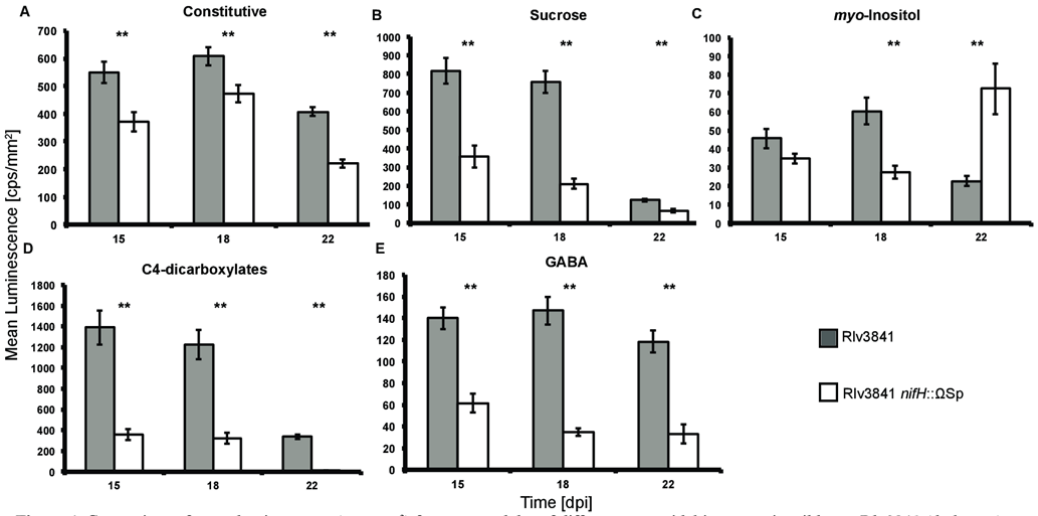

Figure 4. Comparison of mean luminescence (cps mm^{-2}) from pea nodules of different ages with biosensors in wild-type Rlv3841 (dark gray) or Rlv3841 nifH::ΩSp mutant (white) background. Nodules formed by Rlv3841 fix nitrogen whereas those formed by these mutant strains are unable to do so. Biosensors are specific for: constitutively active (A), sucrose (B), myo-inositol (C), C4-dicarboxylates (D) and GABA (E). Standard errors are shown by bars and stars indicate significant differences between a biosensor in wild-type Rlv3841 and the Rlv3841 nifH::ΩSp mutant (t-test, * = p <0.05; ** = p <0.01). Differences between each time point (ANOVA with post hoc Tukey test, p <0.05) are reported in Supplemental Tables S6 and S7.

Expression of the *myo*-inositol reporter that was seen 15 dpi was mostly in nodules. A similar pattern was seen for the reporters detecting xylose (able to detect ≥ 1 mM xylose), fructose (able to detect ≥ 10 μM fructose) and the flavonoid, hesperetin (able to detect ≥ 1 μM hesperetin) (Fig. 3, A-B and F, Supplemental Fig. S5, A-B and F). Biosensors for these compounds were highly expressed in the rhizosphere at 4-8 dpi, usually localized at and above lateral root tips and then, despite a general decrease in luminescence over the whole root, the compounds were then detected almost exclusively in nodules 15-22 dpi (Supplemental Fig. S5, A-B and F). Expression of the organic acid C4-dicarboxylate biosensor indicated that succinate/malate/aspartate (able to detect ≥ 100 μM/ ≥ 10 μM/ ≥ 10 mM of succinate/malate/aspartate, respectively) are present in the rhizosphere and then found specifically localized to nodules at 15-18 dpi, with levels dropping by 22 dpi (Fig 4D, Supplemental Fig. S5C).

A second expression profile, although similar to that described above, is that of biosensors that gave a strong signal on roots but were barely detectable within nodules. For example, the biosensor for malonate (able to detect ≥ 10 mM malonate) (Fig. 2, C and G) was detected only in the rhizosphere (4-8 dpi), both on primary and lateral roots, with the highest levels appearing just before the root tips (Fig. 2C). The expression of this reporter fell over the time course (Fig. 2G) and was barely detectable in early nodules (11-15 dpi) and undetectable in older nodules (18-22 dpi) (Fig. 2, C and G).

A third profile, typified by the phenylalanine biosensor (able to detect ≥ 10 μM phenylalanine), showed two peaks of total luminescence (Fig. 2H) similar to that seen with the constitutive promoter (Fig. 1B), one at 8 dpi with the signal localized to the root elongation zone of lateral roots, and a second peak both in the rhizosphere and in nodules (15 dpi) (Fig. 2, D and H). Although the total signal from the phenylalanine reporter detection fell over time, at 18-22 dpi the luminescence was confined to nodules. By following the pattern of luminescence of a number of individual nodules, we conclude that the phenylalanine concentration peaks in nodules and then falls as the nodule senesces. As new nodules are being initiated constantly over the time course analyzed, there were numerous bright spots, which got brighter as the nodule developed and then faded as nodules got older (Fig. 2D). The tartrate sensor (able to detect levels ≥ 100 μM tartrate), was expressed in a temporal pattern similar to that of phenylalanine with a similar dip in total levels of detection as nodules form 11 dpi (Fig. 3D), although, in contrast to the phenylalanine sensor, the tartrate reporter was expressed largely on the primary root (4-15 dpi) (Supplemental Fig. S5D); there may be low levels of expression of the tartrate reporter in mature nodules (22 dpi) (Supplemental Fig. S5D).

A fourth profile was high expression of the reporter in nodules once they are formed, with very weak or no luminescence in the rhizosphere on pea roots in general prior to that. The biosensor for sucrose typifies this group (Fig. 2, A and E). The total levels of expression of the sucrose reporter (able to detect levels ≥ 100 μM sucrose), did not peak until the nodules were more mature (15-18 dpi) and then fell as the nodules senesced (22 dpi) (Fig. 2E). In the same way, expression of the GABA reporter (able to detect levels ≥ 500 μM GABA), was hardly detected in the rhizosphere, but was induced specifically in nodules, with total levels peaking at 15-18 dpi (Fig. 3E, Supplemental Fig. S5E).

The fifth profile was seen with a group of biosensors that gave results too low to properly evaluate, because luminescence was routinely detected below a mean intensity *per* pixel of approx. 30 (Supplemental Fig. S6). The polyol reporters for erythritol (able to detect levels ≥ 1 mM erythritol), and mannitol (able to detect levels ≥ 1 μM mannitol), were barely detected in either the rhizosphere or in nodules of pea plants (Supplemental Fig. S6, A-B). The reporter for formate (able to detect levels ≥ 10 mM formate), was expressed at very low levels and expression of the salicylic acid

reporter (able to detect levels ≥ 1 mM salicylate), was not detectable (Supplemental Fig. S6, C-D). This last result is not unexpected, because formate and salicylic acid were not found in the metabolomic analysis of pea root exudate (Supplemental Table S3).

Based on the spatial localization on pea roots of the reporters, we can draw conclusions about metabolites found in the rhizosphere prior to nodule formation (Table III). Xylose (≥ 1 mM), fructose (≥ 10 μM), *myo*-inositol (≥100 μM), phenylalanine (≥ 10 μM) and hesperetin (≥ 1 μM) are largely exuded by the elongation zone of primary and lateral roots (Fig. 2, B and D, Supplemental Fig. S5, A-B and F). Malonate (≥ 10 mM) was detected on both the uppermost portion of the primary root and the elongation zone of primary and lateral roots (Fig. 2C). Tartrate (≥ 100 μM) exudation was exclusively localized to the uppermost portion of the primary root, with little or no tartrate being detectable on the lateral roots (Supplemental Fig. S5D). Although present in the pea rhizosphere, the localization of C4-dicarboxylates was not clear, because detection in different regions varied over time with no clear pattern being observed (Supplemental Fig. S5C).

Between 11 and 15 dpi nodules became visible on pea roots. The reporters indicate that xylose (≥ 1mM), fructose (≥ 10 μM), sucrose (≥ 100 μM), *myo*-inositol (≥ 100 μM), C4-dicarboxylates (≥ 10 μM -10 mM, see Table I), phenylalanine ((≥ 10 μM), GABA (≥ 500 μM) and hesperetin (≥ 10 μM) were present in nodules at 15 dpi (Table III, Fig. 2 A, B, D-F, and H, Fig. 4 B-E, and Supplemental Fig. S7). Malonate (≥ 10 mM), and tartrate (≥ 100 μM), were detectable in nodules at 15 dpi, but at very low levels of bio-reporter expression (towards the lower limit of detection) (Table III, Fig. 2 C and G, and Supplemental Fig. S5D). For both phenylalanine and hesperetin, levels were highest in nodules at 15 dpi (dropping to 18 dpi, and dropping further to 22 dpi) (Table III, Supplemental Fig. S5F, and Supplemental Fig. S7, C-D). In most of the biosensors, the signal from nodules was strongly reduced by 22 dpi probably due to the general plant growth conditions, the only exception being the fructose reporter where the signal increased until 22 dpi (Table III and Supplemental Fig. S7B).

Effect of Nodulation on Rhizosphere Metabolites

Since wild-type Rlv3841 induces nodule formation on pea roots, the effects of

nodulation on pea root secretion were investigated by comparing the induction of the biosensors in wild-type with their induction in a mutant unable to induce nodulation (a derivative of Rlv3841 carrying *nodC128*::Tn*5* (Downie et al., 1985)). Rhizobia produce Nod factors enabling recognition by legumes, and *nodC* mutants are unable to enter the plant or induce nodule formation (Udvardi and Poole, 2013). By comparing results obtained with wild-type and mutant backgrounds it is possible to separate the processes and metabolite changes of root colonization and nodule formation (Fig. 2 and 4, Supplemental Fig. S5, S8 and S9). Notably, in the pre-nodule formation stage, 4-8 dpi, no significant differences occurred between any biosensor in the two different backgrounds, other than with the *myo*-inositol reporter 8 dpi (Fig. 2F). This suggests that the presence of Nod factor in itself does not alter either the amount or the localization of root secretions prior to nodule formation for the sugars xylose, fructose, and sucrose, the organic acids malonate, C4-dicarboxylates, and tartrate or the amino acids phenylalanine, and GABA.

With the *nodC* mutant that is unable to form nodules, there was a significant decrease in detection of *myo*-inositol at 8 dpi relative to wild-type (Fig. 2F). In a wild-type strain at this time point, nodule initiation has begun, although nodules are not yet visible to the naked eye. The conclusion that *myo*-inositol (at concentrations ≥ 100 μM) is present in developing and very young nodules can be drawn from the relative decrease in *lux* expression of *myo*-inositol biosensor on roots inoculated with the *nodC* mutant. There was also a significant decrease in expression of the *myo*-inositol reporter in roots inoculated with the *nodC* mutant at each time point from 8 to 18 dpi, suggesting the *myo*-inositol detected in the roots inoculated with wild-type is due to nodule formation (Fig. 2F). Indeed, expression of the *myo*-inositol reporter can be seen clearly localized to nodules (Fig. 2B). Lux output from the sucrose reporter (detecting concentrations ≥ 100 μM sucrose), was reduced significantly at 11-22 dpi in roots inoculated with the *nodC* mutant compared with wild-type (Fig. 2E); the expression of this reporter in roots inoculated with Rlv3841 was clearly seen localized to nodules at 15-22 dpi and this is consistent with sucrose from the shoot being supplied to nodules to support nitrogen fixation by rhizobial bacteroids (Fig. 2A). Expression of the phenylalanine reporter (detecting concentrations of ≥ 10 μM phenylalanine), was reduced significantly only at 15 dpi in roots inoculated with the *nodC* mutant compared to wild-type (Fig. 2H), suggesting phenylalanine is abundant

in nodules of this age. For fructose, C4-dicarboxylates, GABA, and hesperetin bioreporters, levels are significantly lower in the *nodC* mutant background at 18 dpi, 15 dpi, 15 and 18 dpi, and 18 dpi, respectively (Fig. 3, B-C, and E-F), indicating the presence of these metabolites (fructose ≥ 10 μM, C4-dicarboxylates ≥ 10 μM – 10mM, GABA ≥ 500 μM, hesperetin ≥ 1 μM) in pea nodules.

Effect of Symbiotic Nitrogen Fixation on Nodule Metabolites

Biosensors detecting sucrose (sugar), *myo*-inositol (polyol), C4-dicarboxylates (organic acid) and GABA (amino acid) were used to examine levels of metabolites within effective and ineffective nodules by transferring each to a *nifH* mutant background (Karunakaran et al., 2009). The *nifH* mutant induces normal nodule formation, but is totally defective for nitrogen fixation. Since *nifH* encodes one of the components of nitrogenase, the enzyme complex that carries out nitrogen fixation, interruption of this gene by mutation means no functional nitrogenase is produced by the bacteria.

Levels of Lux expression from a constitutive promoter were approx. 30% lower in the Rlv3841 *nifH* mutant background relative to wild-type (Fig. 4A), presumably because ineffective nodules do not contain as many, and/or as metabolically active, bacteroids. Levels of detection of sucrose, *myo*-inositol, C4-dicarboxylates and GABA in effective (wild-type) and ineffective (*nifH* mutant-background) nodules were compared 15, 18, and 22 dpi (Fig. 4, B-E). Once corrected for overall lower activity in the *nifH*-mutant background (Supplemental Fig. S10), lower levels of sucrose (approx. 65% at 15 dpi, approx. 35% at 18 dpi), C4-dicarboxylates (approx. 35% at 15-18 dpi, > 10% at 22 dpi), and GABA (approx. 65% at 15 dpi, approx. 30% at 18 dpi and approx. 50% at 22 dpi) were detected in ineffective nodules. The reduction of sucrose, C4-dicarboxylates and GABA in ineffective nodules suggests that plants sanction nodules that cannot fix nitrogen by decreasing their carbon supply (Fig. 4, B, and D-E). In contrast, the level of *myo*-inositol detected was higher in ineffective senescing nodules at 22 dpi (approx. 600% at 22 dpi) (Fig. 4C, Supplemental Fig. S10).

Malonate catabolism is not required for nitrogen fixation (Karunakaran et al., 2013). Transcriptomic data did not show a significant change in the expression of *matABC* genes in the rhizosphere of pea plants, but a significant difference was found

499 in the alfalfa rhizosphere (Ramachandran et al., 2011). The malonate biosensor
500 indicates that malonate (at concentrations ≥ 10 mM) is present in the pea rhizosphere,
501 although over time its level decreases to being barely detectable in nodules 15 dpi
502 (Fig. 2, C and G). With evidence that ≥ 10 mM malonate is present in the rhizosphere
503 of peas, colonization of roots by *R. leguminosarum* mutants defective for malonate
504 metabolism was explored to see if an inability to metabolize malonate affects this
505 process. Root attachment assays and nodule competition (as a measure of effective
506 root colonization) were assayed using *matC* and *matA* mutants that are impaired in
507 malonate transport and catabolism, respectively (Karunakaran et al., 2013). Although
508 both mutants, defective in either malonate transport or catabolism, are less efficient at
509 root attachment than the wild-type, there were no significant differences in pea root
510 colonization compared with wild-type (Supplemental Fig. S11). We conclude from
511 this that malonate uptake and its subsequent bacterial catabolism play a part in the
512 initial attachment of *R. leguminosarum* to pea roots. However, although attachment
513 might be the first step of bacterial colonization, in overall colonization assays, ability
514 to either take-up or metabolize malonate has no effect.

515 ***In vivo* Mapping of Metabolites on Roots and within Nodules of *V. hirsuta***

516 To investigate a different legume root and its rhizosphere, similar analyses
517 were performed with *V. hirsuta,* on which Rlv3841 is also able to form nodules.
518 Images were acquired at similar time points as for pea (up to 22 dpi), but with vetch
519 plants the nodules appear to the naked eye earlier, at about 8 dpi (Fig. 5 and Table
520 IV). With the exception of the polyols, erythritol and mannitol, and the organic acids,
521 formate, tartrate and salicylic acid, all other metabolite were detected in the vetch
522 rhizosphere over the time course (Table IV). For the compounds we failed to detect,
523 we can't exclude the possibility that they may be present, but at levels too low for
524 their detection, i.e. levels of erythritol at ≤ 1 mM, mannitol at ≤ 1 μM, formate at ≤ 10
525 mM, tartrate at ≤ 100 μM and salicylic acid at ≤ 1 mM. This differs from pea only in
526 the case of the tartrate, which was detected in the pea rhizosphere but not in that of
527 vetch. Metabolites xylose (≥ 1 mM), fructose (≥ 10 μM), *myo*-inositol (≥ 100 μM),
528 malonate (≥ 10 mM), C4-dicarboxylates (≥ 10 μM -10 mM, Table I), and hesperetin
529 (≥ 1 μM) were detected in the vetch rhizosphere at 4 dpi (Fig. 5, A-B, D-F, and I).
530 These were also all detected on pea roots (Table III), but a difference between these
531 two legume rhizospheres is that phenylalanine was barely detected in the vetch

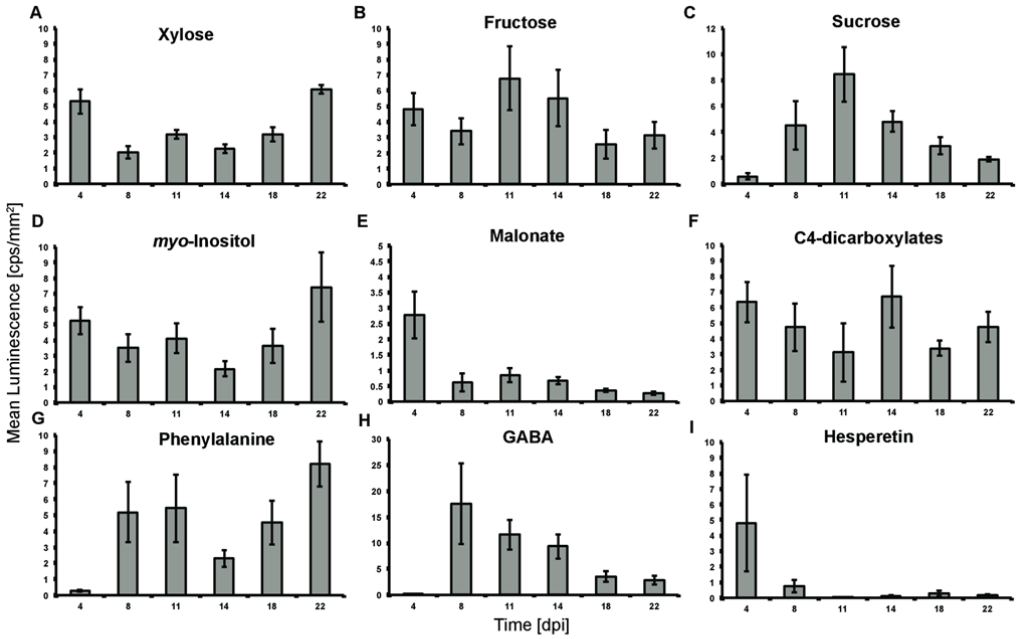

Figure 5. Comparison of mean luminescence (cps mm-2) from vetch roots inoculated with biosensors in wild-type Rlv3841 background. Biosensors detect: xylose (A), fructose (B), sucrose (C), myo-inositol (D), malonate (E), C4-dicarboxylates (F), phenylalanine (G), GABA (H) and hesperetin (I). Standard errors are shown by bars. Differences between each time point (ANOVA with post hoc Tukey test, $p < 0.05$) are reported in Supplemental Table S8. Nodules are visible to the naked eye from 8 dpi.

rhizosphere at 4 dpi (Fig. 5G) (the limit of detection is ≥ 10 µM phenylalanine). In vetch, as in pea, sucrose (able to detect ≥ 100 µM), and GABA (able to detect (≥ 500 µM) were hardly detected on the roots prior to nodule formation but were detected within nodules: for sucrose, the maximum level was observed at 11 dpi, while that of GABA peaked at 8 dpi (Fig. 5, C and H). This pattern is similar overall to that seen on pea roots for both sucrose (Fig. 2E) and GABA (Fig. 3E), taking into account that pea nodules form later (>11 dpi). Malonate (≥ 10 mM) was detected in the vetch rhizosphere prior to nodule formation, but once nodules were formed (> 8 dpi), it was detected only at a very low level (8-22 dpi) (Fig. 5E), again, a similar pattern to that of pea (Fig. 2G). Hesperetin (≥ 1 µM) was detected in vetch, with levels peaking at 4 dpi, and then falling once nodule development was initiated (8 dpi onwards) (Fig. 5I). Images from 1-22 dpi for detection of hesperetin on vetch roots (Fig. 6) show that, even at 1-4 dpi, prior to any sign of nodule formation, there are foci where hesperetin is detected. At later time points, nodules developed at these exact locations illustrating the power of this technique in pinpointing the spatial and temporal secretion of this flavonoid (Fig. 6).

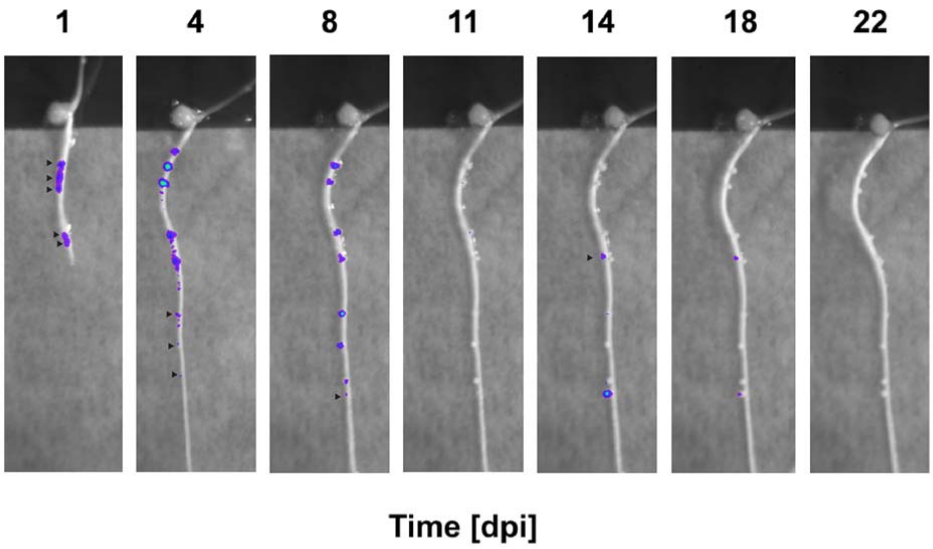

Figure 6. Time-course of hesperetin detection on a vetch seedling root from 1 to 22 dpi. Arrows indicate spots where luminescence is concentrated and a nodule forms later.

DISCUSSION

Owing to the hidden nature of the rhizosphere and its complexity, a major problem encountered in its study is the intrinsic difficulty in sampling (Bais et al., 2006). Most of the techniques used require either sacrifice of the specimen, or at least require its manipulation, making it impossible to non-invasively follow the same sample over time. The bacterial *lux* gene cassette has been widely used in several different applications, including the visualization of gene expression, as a tool for cellular population monitoring and as bioreporter target through activation under specific, predetermined conditions (Close et al., 2012). In this work, we have constructed a suite of Lux biosensors able to detect a variety of key sugars, polyols, organic acids, amino acids and flavonoids that are commonly found in root exudates. The presence of these compounds was confirmed using a metabolomics approach, allowing us to identify 376 compounds present in pea root exudate. Lux-based reporter plasmids have been transferred into Rlv3841, an alpha-proteobacterium, which is generally associated with leguminous plants and is ubiquitous in soil (Udvardi and Poole, 2013). Pea and vetch plants, both hosts of *R. leguminosarum,* on which it forms nitrogen-fixing nodules, have been used to test the efficiency of this system as a proof-of-concept. However, the ability of rhizobia to colonize non-legume plants (Chabot et al., 1996) should allow the use of these bioreporters in other systems.

A constitutive promoter was used to examine rhizobial colonization of plant

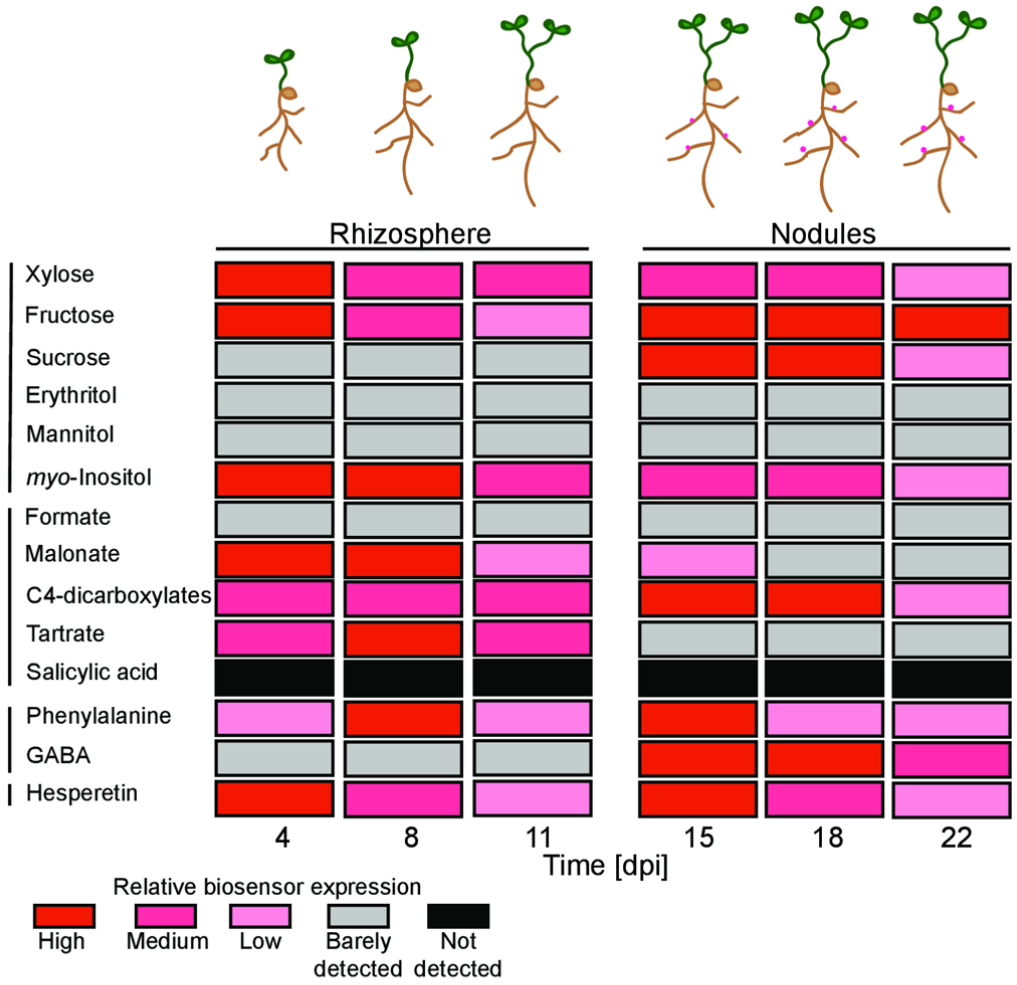

Figure 7. Summary of metabolite detection on pea roots; in the rhizosphere (≤11 dpi) and within nitrogen-fixing nodules (≥15 dpi). Lines on the left-hand side group similar chemicals into; sugars and polyols, organic acids, amino acids, and flavonoids. Color shows level detected in rhizosphere and nodules: high, red; medium, dark pink; low, pale pink; barely detected, gray; not detected, black.

roots. Bacteria colonize the whole of the root system but the strongest Lux signals are visible from the elongation zone of the primary and lateral roots (Fig. 1, Supplemental Fig. S2). Heavy colonization at the root elongation zone is to be expected, as this is an area of actively growing root where many metabolites are secreted and exuded. Low Lux signal from the root cap is probably due to the reduced colonization of this area, which generally secretes antimicrobial phytochemicals (Baetz and Martinoia, 2014). The level of Lux signal detected in the rhizosphere was constant until 11 dpi and then reduced, possibly due to a general decrease in root exudation caused by plant growth conditions and/or to the physiological status of the bacterial population. Constitutive *lux* expression drains energy reserves in bacterial cells and reduces the light output over time. In a wild-type bacterial background, after 11 dpi the Lux signal was mainly localized in the nitrogen-fixing nodules formed on the legume roots which is densely

populated with metabolically active bacteria. It is important to consider where bacteria are located. Although the whole root is colonized by rhizobia (Figure S2), these are unevenly distributed i.e. more bacteria or more metabolically active bacteria are in the root elongation zone. The overall levels of metabolites detected in the rhizosphere before 11 dpi and in nodules (after 11 dpi) for pea roots are summarized in Fig. 7.

On pea and vetch roots, xylose (≥ 1 mM), fructose (≥ 10 μM), *myo*-inositol (≥ 100 μM), phenylalanine (≥ 10 μM) (not detected in the vetch rhizosphere), and hesperetin (≥ 1 μM) were detected largely at the elongation zone (just behind the root tip) of lateral roots, while malonate (≥ 10 mM) (at least initially) and tartrate (≥ 100 μM) (not detected on vetch roots) were mainly localized on the primary root (Fig. 2C and Supplemental Fig. S5D). In Rlv3841, malonate transport and metabolism has been shown to have no role in nitrogen fixation in peas (Karunakaran et al., 2013), but does seem to be involved in attachment of Rlv3841 to pea roots as mutants in malonate uptake and metabolism show a reduced attachment phenotype, although no change in overall colonization of pea roots is observed. Malonate at ≥ 10 mM is localized to the primary root at 4 dpi during initial colonization (although levels of ≤ 10 mM malonate may well be present on other parts of the root but are below the levels of detection by this method). Given the role of malonate in attachment, it is possible that bacteria attach to the primary root before colonizing the lateral roots, where most of the nodules subsequently appear. C4-dicarboxylates (succinate/malate/aspartate with detection levels ≥ 100 μM/ ≥ 10 μM/ ≥ 10 mM, respectively) were detected in the rhizosphere of both pea and vetch, but showed no clear spatial pattern on pea roots (Supplemental Fig. 3C).

In pea and vetch nodules, xylose (≥ 1 mM), fructose (≥ 10 μM), sucrose (≥ 100 μM), *myo*-inositol (≥ 100 μM), C4-dicarboxylates (succinate/malate/aspartate, (≥ 10 μM – 10 mM), phenylalanine (≥ 10 μM), and GABA (≥ 500 μM) were present (Table III, Table IV, Fig. 7). Although nodules formed on pea and vetch have not been analyzed by metabolomic studies, MALDI mass spectrometric analysis of *Medicago truncatula* nodules formed by *S. meliloti* (Ye et al., 2013) revealed many of these same compounds present: sucrose, C4-dicarboxylates (succinate/malate/ aspartate), and GABA, but also salicylic acid was detected, which, if present in pea or vetch nodules, is below the limits of detection (≤ 1 mM) of Lux-based salicylic acid

616 detection. In pea, hesperetin (≥ 1 μM) was detected in mature nodules (Fig. 3F), while
617 in vetch it was detected only before nodules could be seen with the naked eye or in
618 very young nodules, with none detected in mature nodules (i.e. levels ≤ 1 μM) (Fig.
619 6). Sucrose is supplied from the shoot to nodules, where it is converted to C4-
620 dicarboxylates and supplied to bacteroids as their primary energy source for nitrogen
621 fixation (Poole and Allaway, 2000). In the ineffective nodules of a *nifH*-mutant
622 background, the levels of sucrose and C4-dicarboxylates detected were lower,
623 suggesting that the plant sanctions supply of carbon to nodules unable to provide them
624 with nitrogen. While the *nifH*-mutant showed lower levels of the constitutive
625 promoter, presumably because of reduced bacteroid numbers and metabolic activity,
626 (Kiers et al., 2003; Berrabah et al., 2015), the levels of sucrose, C4-dicarboxylates and
627 GABA were still substantially reduced when the decrease in activity of the
628 constitutive promoter was accounted for. Furthermore, levels of some metabolites,
629 such as *myo*-inositol, increased dramatically in the *nifH* mutant possibly due to
630 environmental/osmotic stress.
631 Use of these tools has allowed us to draw a spatial and temporal map of key
632 compounds present in the legume rhizosphere and to monitor the relative supply of
633 specific metabolites inside nodules (e.g. sucrose, C4-dicarboxylates, GABA). We
634 have demonstrated that with this system it is possible to follow the same plant for
635 days, gathering data non-invasively and it is relatively easy to set up. Moreover, it
636 will be possible in the future to expand the set of reporters to include many different
637 compounds. We believe that this is an excellent tool, which can be adapted to
638 investigate the role of specific root exudates in many different plant growth
639 conditions (e.g. stress; both abiotic and biotic). As *R. leguminosarum* spp. colonize
640 root systems of non-leguminous plants (Schloter et al., 1997), it will be possible to
641 monitor root exudates of other plant species using this series of biosensors. By
642 combining this methodology with plant mutant collections, screening specific
643 exudate-related phenotypes in genome-wide association studies could be performed.
644 Finally, by co-inoculating biosensors with other bacteria and/or fungi, it will be
645 possible to observe the effects of other microorganisms on the plant secretome.
646

647 # MATERIALS AND METHODS

Bacterial Strains and Growth Conditions

The bacterial strains and plasmids used in this study are listed in Supplemental Table S1. *Escherichia coli* strains were grown in liquid or solid Luria–Bertani (LB) medium (Sambrook et al., 1989) at 37°C supplemented with appropriate antibiotics: tetracycline (10 μg ml^{-1}) and kanamycin (20 μg ml^{-1}). Rlv3841 carrying *nodC128*::Tn5 was isolated by transduction using phage RL38 propagated on strain 6015 carrying *nodC128*::Tn5 on pRL1JI (Downie et al., 1985). Rlv3841 strains were grown in tryptone yeast (TY) agar or broth (Beringer, 1974) or universal minimal salts (UMS) at 28°C. UMS is derived from AMS (Poole et al., 1994) with the changes being: EDTA-Na_2 (1 μM), $CoCl_2.6H_2O$ (4.2 μM), $FeSO_4.7H_2O$ (0.04 mM) and $CaCl_2.2H_2O$ (0.51 mM); UMS was supplemented with 30 mM pyruvate and 10 mM ammonium chloride as the carbon and nitrogen sources, unless otherwise stated (Supplemental Table S2). UMA is UMS with the addition of 16 g l^{-1} agar. Antibiotics were added when necessary at the following concentrations: streptomycin (500 μg ml^{-1}), tetracycline (2 μg ml^{-1} in UMS, 5 μg ml^{-1} in TY), spectinomycin (100 μg ml^{-1}) and neomycin (20 μg ml^{-1}).

Strain Construction and General Techniques

The promoter region (often including the complete upstream regulator) of each of the candidate genes was amplified using primers listed in Supplemental Table S9 with Phusion High-Fidelity DNA Polymerase (ThermoFischer, Waltham, MA, USA) according to manufacturer's instructions. Fragments were purified and double digested with *Kpn*I or *Xho*I (at the 5′-end) and *Xh*oI or *Bam*HI (at the 3′-end) (ThermoFischer). Restriction fragments were cloned into pIJ11268 (Frederix et al., 2014) digested with the same enzymes. Plasmids (Supplemental Table S1) were transferred into wild-type (Rlv3841), Rlv3841 *nodC128*::Tn5, Rlv3841 *nifH*::ΩSp (Karunakaran et al., 2009), Rlv3841 *matA*::pK19 and Rlv3841 *matC*::pK19 (Karunakaran et al., 2013) backgrounds by tri-parental mating according to Figurski and Helinski (Figurski and Helinski, 1979). All plasmids are available from addgene (https://www.addgene.org).

Determining Solute Specificity

Each biosensor was grown for 3 d on an UMA slope with antibiotics, re-suspended in UMS with no added carbon or nitrogen and washed three times. Each was then diluted to an OD_{600} of 0.01 in a final volume of 5 ml UMS with a sugar (10 mM) as sole carbon source, or with pyruvate (30 mM) as carbon source in presence of a specific compound (Supplemental Table S2) for 17 h. Luminescence (in relative luminescence units (RLU)) and OD_{600} were measured using a GloMax®-Multi+ Detection System (Promega, Fichburg, WI, USA). For each compound, the fold-induction is defined as the ratio of RLU/OD_{600}, when grown in the presence of that compound (Supplemental Table S2 gives concentrations of each solute), with that obtained in control conditions (UMS with pyruvate and ammonia). The solute(s) that give the highest fold-induction and specific luminescence (Table I) are described as inducer(s). Biosensor induction by a solute is described as specific if the specific luminescence is ≥10-fold that observed from the other solutes tested. The biosensors for erythritol, formate, and GABA have a relatively high expression with a variety of non-related solutes (background) and they are described as being specific for these solutes, respectively, with specific luminescence ≥4-fold values obtained with other solutes. More than one compound is considered inducing when the fold-induction is > 40% of the maximum fold-induction for a biosensor (Table I). For each biosensor grown on each solute, three independent cultures were measured. Supplemental Table S10 shows the expression of each gene used in biosensor construction in microarray experiments performed under seventy-three different conditions.

Plant Growth Conditions

Seeds of *Pisum sativum* cv Avola and *Vicia hirsuta* were surface sterilized and germinated on distilled water agar plates. Plates with pea seedlings were put into black bags and incubated for 6 d at room temperature. Vetch seedlings were incubated overnight at 4°C and for 3 d at room temperature. Seedlings were transferred to 10-cm square Petri dishes containing FP agar (Somasegaran and Hoben, 1994) covered with sterile filter paper (one seedling per plate for peas, six per plate for vetch). Each biosensor was analyzed with at least 4 plates for pea (corresponding to 4 plants) and 1 plate for vetch (corresponding to 6 plants). Biosensors were grown on UMA slopes for 3 d at 27°C, washed 3 times in UMS without any additions and inoculated directly on the seedling root. Each seedling was inoculated with 5×10^7 or 2×10^7 colony forming units (cfu), for vetch and pea plants, respectively. Plates were covered with

aluminum foil to prevent exposure of roots to light and placed in a growth chambers at 23°C with a 16 h/8 h day/night for 22 d. In flooding experiments, peas were grown for 4 dpi with a biosensor before the plate was flooded with 10 ml of 10 mM solution of substrate and poured off. Plates were imaged before, and 5 min, 3 hr, and 21 hr post-flooding. Background luminescence in experiments with plants was evaluated by spotting 2 x 10^7 cfu ml^{-1} bacteria (the same amount used for pea root inoculation) onto FP plates supplemented with pyruvate and ammonium chloride. Plates were imaged after 7 d.

Image Acquisition

Plates were photographed using a NightOWL camera (Berthold Technologies, Bad Wildbad, Germany) 4, 8, 11, 15, 18, and 22 d post inoculation (dpi). CCD images of light output were exposed for 120 s. Each CCD image consisted of an array 1024 by 1024 pixels, and after acquisition pictures were post-processed for cosmic suppression and background correction. Images were analyzed with the imaging software IndiGO (Berthold Technologies) and with the custom software, NightCROP. NightCROP first segments an image using the SeNeCA algorithm (Tomek et al., 2013) into roots and background using a bright-field image, discarding objects smaller than 1000 pixels. All subsequent analysis uses the respective fluorescence image. The script subtracts background intensity: background in the image is defined as a set of pixels given by logical inverse of the mask containing roots, subsequently morphologically eroded with a disk structural element of radius 9 to filter out signal from the edges of roots. Then, for each pixel belonging to a root, mean intensity of background pixels in a 200-by-200-pixel square is subtracted. The output from NightCROP for a given image is expressed as mean intensity of pixels labeled as roots after the background subtraction. Exact values of parameters (minimum root size, erosion radius and background size) may be freely selected, based on the resolution and nature of data (Fig. S1). Data are expressed as the ratio of luminescence/surface; cps mm^{-2} (counts per second mm^{-2}; IndiGO) or intensity pxl^{-1} (NightCROP).

Software Development and Use

NightCROP was developed as a script for MATLAB environment (MATLAB version 8.5.0 r2015a, (MathWorks Inc., Natick, MA, USA)). Before using the script

749 an image processing toolbox should be installed in MATLAB. The script is available
750 upon request to the corresponding author and works on any operating system which
751 supports MATLAB.
752
753 **Extraction of Exudate from Roots**
754 Glass jars (0.5 l) were prepared by filling one third of the jar with glass beads
755 (6 mm diameter; Atlas Ball & Bearing Co. Ltd., Walsall, UK) and adding water
756 (reverse osmosis highest quality) to cover all except the top layer of beads (approx.
757 150 ml). Jars were covered with a metal lid containing a foam bung and sterilized by
758 autoclaving. Six sets of twenty sterilized and germinated peas with 1 cm roots were
759 transferred into six sterilized glass jars, with each jar (of twenty plants) representing
760 one biological replicate. The jars were wrapped with black plastic up to the level of
761 the beads and the peas grown for 21 d at 20^{o}C for 16 h light /18^{o}C for 8 h dark. The
762 liquid was then decanted into sterile glass bottles and sampled for sterility by plating
763 100 µl aliquots on TY plates. Samples were filtered through a 0.2-µm nitrocellulose
764 filter. Samples for metabolite profiling were freeze- dried and re-suspended in 800 µl
765 of sterile water prior to downstream analysis.
766
767 **Metabolite Profiling Analysis**
768 The metabolomic profile of six biological replicates of pea root exudates was
769 analyzed using non-biased, global metabolome profiling technology based on GC/MS
770 and UHLC/MS/MS^2 platforms (Lawton et al., 2008; Evans et al., 2009; Terpolilli et
771 al., 2016) developed by Metabolon (www.metabolon.com). Samples from the six
772 biological replicates were extracted using the automated MicroLab STAR® system
773 (Hamilton, www.hamiltoncompany.com). Recovery standards (Evans et al., 2009)
774 were added prior to the first step in the extraction process for QC purposes. The
775 protein fraction was removed using methanol extraction, which allows maximum
776 recovery of small molecules. The resulting extract was divided into two fractions: one
777 for analysis by LC and one for analysis by GC. Organic solvent was removed by
778 placing samples on a TurboVap® (Zymark). Each sample was frozen and dried under
779 vacuum. Samples were then prepared for the appropriate instrument, either LC/MS or
780 GC/MS.
781 The LC/MS portion of the platform was based on a Waters ACQUITY
782 UHPLC and a Thermo-Finnigan LTQ mass spectrometer, which consisted of an

783 electrospray ionization source and linear ion-trap mass analyzer. The sample extract
784 was split into two aliquots, dried and then reconstituted in acidic or basic LC-
785 compatible solvents, each of which contained 11 or more injection standards at fixed
786 concentrations. One aliquot was analyzed using acidic positive ion optimized
787 conditions and the other using basic negative ion optimized conditions in two
788 independent injections using separate dedicated columns. Extracts reconstituted in
789 acidic conditions were gradient-eluted using water and methanol both containing
790 0.1% (v/v) formic acid, while the basic extracts, which also used water/methanol,
791 contained 6.5 mM NH_4HCO_3. The MS analysis alternated between MS and data-
792 dependent MS^2 scans using dynamic exclusion.
793 Samples destined for GC/MS analysis were re-dried under vacuum desiccation
794 for a minimum of 24 h prior to being derivatized under dried nitrogen using
795 bistrimethyl-silyl-triflouroacetamide. The GC column was 5% phenyl and the
796 temperature ramp was 40°C to 300°C, over a 16-min period. Samples were analyzed
797 on a Thermo-Finnigan Trace DSQ fast-scanning single-quadrupole gas
798 chromatograph mass spectrometer using electron impact ionization. For metabolite
799 profiling, identification of known chemical entities was based on comparison to
800 metabolomic library entries of purified standards as previously described (Evans et
801 al., 2009; Yobi et al., 2012).
802
803 **RNA Isolation and Microarray Analysis**
804 Rlv3841 was grown overnight in 10 ml of UMS supplemented with
805 pyruvate/ammonia. Cultures were split in two and concentrated root exudates (5
806 mg/ml) were added to one culture. After 3 h of induction RNA was extracted from
807 three biological replicates, amplified and hybridized as previously described
808 (Karunakaran et al., 2009). Microarray data were deposited in the ArrayExpress
809 database (www.ebi.ac.uk/arrayexpress) under accession number E-MTAB-4790.
810
811 **Root Attachment Assay**
812 Surface-sterilized pea seeds were germinated on distilled water agar plates for
813 5 d. Bacteria were grown on UMA slopes for 3 d, re-suspended and washed twice in
814 phosphate-buffered saline and then 10 ml of a suspension (OD_{600} = 0.1) was added to
815 50 ml glass tubes containing 7-10 pea roots. Tubes were incubated on a rocking
816 platform for 1 h at room temperature at 50 rpm. Roots were washed by dipping six

817 times in PBS and then individual roots were transferred into a 1.5 ml tube, weighed
818 and their luminescence measured using a GloMax®-Multi Jr Single-Tube Multimode
819 Reader (Promega). Luminescence was scored as relative light units. Data are the
820 average of individual roots from at least 3 different experiments; relative light units
821 (RLU) were normalized for the weight of the roots and the average luminescence of
822 roots incubated with bacteria not expressing the *lux* cassette (LMB542) was
823 subtracted. Luminescence of the pure culture after 1 h was used to calculate the
824 relative luminescence of a single bacterial cell. Differences between the three groups
825 were calculated by one-way ANOVA with post hoc Tukey test.
826
827 **Root Competition Assay**
828 Pea plants were grown on FP plates as described above (Plant Growth
829 Conditions), with the addition of a wet filter paper to cover the roots. Strains were co-
830 inoculated in 1:1 ratio (1 x 10^7 cfu of each strain), using combinations of Rlv3841
831 with either Rlv3841 [pIJ11282] or Rlv3841 *matC*::pK19 [pIJ11282] and Rlv3841
832 *matC*::pK19, with either Rlv3841[pIJ11282] or Rlv3841 *matC*::pK19 [pIJ11282]. At
833 7 dpi, plants were imaged using a NightOWL camera and processed using the
834 NightCROP script.
835
836 **Biosensor Sensitivity Assay**
837 Bacterial biosensors from UMA slopes (with appropriate antibiotics) grown
838 for 3 d at 28°C, were washed three times before re-suspension in 3 ml UMS. Bacteria
839 were added to 50 ml of molten (cooled to 42°C) UMA, to give a final concentration of
840 1x 10^8 cfu ml^{-1}. The agar containing bacteria was then poured into a 12-cm square
841 Petri dish and allowed to set. 25 µl droplets (n=5) of 10-fold dilutions of solute,
842 concentrations ranging from 10 mM to 1 µM (including a distilled water control)
843 were spotted onto the agar and incubated at 28°C. Sensitivity of each biosensor was
844 defined as the lowest concentration of solute which gave a signal when imaged using
845 a NightOWL camera at 4 h post-spotting.
846

847 # ACKNOWLEDGEMENTS

848 We would like to acknowledge the technical assistance of Elisabeth Nowak in
849 this work.

850

Figure Legends

Figure 1. *In vivo* spatial and temporal mapping images of pea root colonization and nodulation with wild-type Rlv3841 luminescently-labelled with a constitutive neomycin phophotransferase promoter controlling Lux expression in pIJ11282 (Frederix et al., 2014). A, Images were acquired at 4, 8, 11, 15, 18 and 22 dpi, with nodules visible to the naked eye at between 11 and 15 dpi (scale: 300-12,000 cps). B, Mean luminescence (pxl mm^{-2}) with standard errors shown by bars.

Figure 2. *In vivo* spatial and temporal mapping images of pea roots with biosensors detecting: sucrose (A) (scale: 200-65,535 cps), *myo*-inositol (B) (scale: 150-5,000 cps), malonate (C) (scale: 50-2,000 cps), and phenylalanine (D) (scale: 150-15,000 cps). Images were acquired at 4, 8, 11, 15, 18 and 22 dpi, with nodules visible to the naked eye between 11 and 15 dpi. These images are representative of those from biosensors in wild-type Rlv3841 background which nodulates peas.
Comparison of mean luminescence intensity *per* pixel from pea roots inoculated with biosensors in wild-type Rlv3841 background (dark gray) and Rlv3841 *nodC128*::Tn*5* background (light gray). Only wild-type Rlv3841 can form nodules. The biosensors detect: sucrose (E), *myo*-inositol (F), malonate (G) and phenylalanine (H). Standard errors are shown by bars, stars indicate significant differences between a biosensor in wild-type Rlv3841 and Rlv3841 *nodC128*::Tn*5* backgrounds (t-test, * = $p < 0.05$; ** = $p < 0.01$). Differences between each time point (ANOVA with post hoc Tukey test, $p < 0.05$) are reported in Supplemental Tables S4 and S5. For representative images from Rlv3841 *nodC128*::Tn*5* background see Supplemental Fig. S8.
Close-up light-field photograph and luminescence of roots showing nodules at 15 dpi inoculated with biosensors detecting: sucrose (I), *myo*-inositol (J), malonate (K), and phenylalanine (L).

Figure 3. Comparison of mean luminescence intensity *per* pixel from pea roots inoculated with biosensors in wild-type Rlv3841 (dark gray) or the Rlv3841 *nodC128*::Tn*5* mutant (light gray). Only wild-type Rlv3841 can form nodules. Biosensors detect: xylose (A), fructose (B), C4-dicarboxylates (C) tartrate (D), GABA (E) and hesperetin (F). Standard errors are shown by bars, stars indicate significant differences between a biosensor in wild-type Rlv3841 and Rlv3841 *nodC128*::Tn*5* (t-

884 test, * = p <0.05; ** = p <0.01). Differences between each time point (ANOVA with
885 post hoc Tukey test, p<0.05) are reported in Supplemental Tables S4 and S5. For
886 representative images from Rlv3841 and Rlv3841 *nodC128*::Tn*5* background see
887 Supplemental Figs. S5 and S9, respectively.
888
889 **Figure 4**. Comparison of mean luminescence (cps mm^{-2}) from pea nodules of
890 different ages with biosensors in wild-type Rlv3841 (dark gray) or Rlv3841
891 *nifH*::ΩSp mutant (white) background. Nodules formed by Rlv3841 fix nitrogen
892 whereas those formed by these mutant strains are unable to do so. Biosensors are
893 specific for: constitutively active (A), sucrose (B), *myo*-inositol (C), C4-
894 dicarboxylates (D) and GABA (E). Standard errors are shown by bars and stars
895 indicate significant differences between a biosensor in wild-type Rlv3841 and the
896 Rlv3841 *nifH*::ΩSp mutant (t-test, * = p <0.05; ** = p <0.01). Differences between
897 each time point (ANOVA with post hoc Tukey test, p <0.05) are reported in
898 Supplemental Tables S6 and S7.
899
900 **Figure 5.** Comparison of mean luminescence (cps mm^{-2}) from vetch roots inoculated
901 with biosensors in wild-type Rlv3841 background. Biosensors detect: xylose (A),
902 fructose (B), sucrose (C), *myo*-inositol (D), malonate (E), C4-dicarboxylates (F),
903 phenylalanine (G), GABA (H) and hesperetin (I). Standard errors are shown by bars.
904 Differences between each time point (ANOVA with post hoc Tukey test, p <0.05) are
905 reported in Supplemental Table S8. Nodules are visible to the naked eye from 8 dpi.
906
907 **Figure 6.** Time-course of hesperetin detection on a vetch seedling root from 1 to 22
908 dpi. Arrows indicate spots where luminescence is concentrated and a nodule forms
909 later.
910
911 **Figure 7.** Summary of metabolite detection on pea roots; in the rhizosphere (≤11 dpi)
912 and within nitrogen-fixing nodules (≥15 dpi). Lines on the left-hand side group
913 similar chemicals into; sugars and polyols, organic acids, amino acids, and flavonoids.
914 Color shows level detected in rhizosphere and nodules: high, red; medium, dark pink;
915 low, pale pink; barely detected, gray; not detected, black.
916
917

Supplemental Data

The following supplemental data are available

Supplemental Figure S1. Workflow of the NightCROP image processing script, the picture is a pea inoculated with a constitutively expressed bioreporter at 15 dpi.

Supplemental Figure S2. *In vivo* spatial and temporal mapping images of pea root colonization and nodulation with wild-type Rlv3841.

Supplemental Figure S3. Luminescence is not detected in the absence of plant roots.

Supplemental Figure S4. *In vivo* spatial and temporal mapping images of pea roots inoculated with the xylose biosensor.

Supplemental Figure S5. *In vivo* spatial and temporal mapping images of pea roots with biosensors detecting: sugars, xylose and fructose.

Supplemental Figure S6. Comparison of pea roots inoculated with biosensors in wild-type Rlv3841 and Rlv3841 *nodC128*::Tn*5* mutant background.

Supplemental Figure S7. Comparison of mean luminescence (cps mm^{-2}) of pea nodules from 15 to 22 dpi, with biosensors in wild-type Rlv3841 background.

Supplemental Figure S8. *In vivo* spatial and temporal mapping images of pea roots with biosensors detecting: sucrose, *myo*-inositol, malonate and phenylalanine.

Supplemental Figure S9. *In vivo* spatial and temporal mapping images of pea roots with biosensors detecting: sugars, xylose and fructose, organic acids, C4-dicarboxylates and tartrate, amino acid, GABA and flavonoid, hesperetin.

Supplemental Figure S10. Comparison of mean luminescence (cps mm^{-2}) from pea roots inoculated with biosensors in wild-type Rlv3841 background (dark gray) and Rlv3841 *nifH*::ΩSp mutant background (white).

Supplemental Figure S11. Investigation of the role of malonate during root attachment.

Supplemental Table S1. Strains and plasmids used in this work. St (streptomycin), Neo (neomycin), Tc (tetracycline) and Sp (spectinomycin).

Supplemental Table S2. Conditions used to test specificity the bioreporter library.

Supplemental Table S3. Metabolomic data from root exudates of *P. sativum.*

Supplemental Table S4. ANOVAs with post hoc Tukey test ($p < 0.05$) on total luminescence for bioreporters in Rlv3841 inoculated onto pea plants (Fig. 2 and 3).

950 **Supplemental Table S5.** ANOVAs with post hoc Tukey test ($p < 0.05$) on total
951 luminescence for bioreporters in Rlv3841 *nodC128*::Tn*5* inoculated onto pea plants
952 (Fig. 2 and 3).
953 **Supplemental Table S6.** ANOVAs with post hoc Tukey test ($p < 0.05$) on nodules
954 luminescence for bioreporters in Rlv3841 inoculated onto pea plants (Fig. 4).
955 **Supplemental Table S7.** ANOVAs with post hoc Tukey test ($p < 0.05$) on nodules
956 luminescence for bioreporters in Rlv3841 *nifH*::ΩSp inoculated onto pea plants (Fig.
957 4).
958 **Supplemental Table S8.** ANOVAs with post hoc Tukey test ($p < 0.05$) on total
959 luminescence for bioreporters in Rlv3841 inoculated onto vetch plants (Fig. 5).
960 **Supplemental Table S9.** Primers used in this work.
961 **Supplemental Table S10.** Relative expression in microarray experiments under
962 seventy-three different conditions of the *R. leguminosarum* genes whose promoters
963 were used for construction of biosensors.

964

965 **Supplemental Figure S1.** Workflow of the NightCROP image processing script, the
966 picture is a pea inoculated with a constitutively expressed bioreporter at 15 dpi. A,
967 NightOWL output photographic image of the pea root system. B, NightOWL output
968 luminescent image of same area captured in A. C, NightOWL superimposed image of
969 pictures A and B with false colors. D, NightCROP segmentation of picture A, the
970 program detects difference in light intensity and draws a segmentation mask over the
971 root system. E, Segmentation mask is applied on picture B and luminescence intensity
972 is specifically extracted from the segmented area (pxl/mm^2). F, Mean background
973 luminescence is calculated around each segmented pixel and, subtracting this from the
974 intensity value of the pixel.

975

976 **Supplemental Figure S2.** *In vivo* spatial and temporal mapping images of pea root
977 colonization and nodulation with wild-type Rlv3841 luminescently-labelled with a
978 constitutive neomycin phophotransferase promoter controlling Lux expression in
979 pIJ11282 (Frederix et al., 2014). Images were acquired at 4, 8, 11, 15, 18 and 22 dpi,
980 with nodules visible to the naked eye at between 11 and 15 dpi (scale: 50-12,000 cps).

981

982 **Supplemental Figure S3.** Luminescence is not detected in the absence of plant roots.
983 Luminescence of biosensors on FP media supplemented with pyruvate and
984 ammonium chloride after 7 days' growth (scale: 50-1,000 cps).

985

986 **Supplemental Figure S4.** *In vivo* spatial and temporal mapping images of pea roots
987 inoculated with the xylose biosensor, flooded with xylose at 4 dpi (A); the sucrose
988 biosensor, flooded with sucrose at 4 dpi (B); the GABA biosensor, flooded with
989 GABA at 4 dpi (C); the sucrose biosensor, flooded with GABA at 4 dpi (D) and the
990 GABA biosensor, flooded with sucrose at 4 dpi (E) (scale: 500-5,000 cps). For each,
991 images were taken before, and 5 min, 3 hr, and 21 hr post-flooding.

992

993 **Supplemental Figure S5.** *In vivo* spatial and temporal mapping images of pea roots
994 with biosensors detecting: sugars, xylose (A) (scale: 400-12,000 cps) and fructose (B)
995 (scale: 300-12,000 cps), organic acids, C4-dicarboxylates (C) (scale: 400-65,535 cps)
996 and tartrate (D) (scale: 200-15,000 cps), amino acid, GABA (E) (scale: 500-10,000
997 cps) and flavonoid, hesperetin (F) (scale: 250-13,000 cps). Images were acquired at 4,

8, 11, 15, 18 and 22 dpi with nodules visible to the naked eye at between 11 and 15 dpi. These images are representative of those from biosensors in wild-type Rlv3841 background.

Supplemental Figure S6. Comparison of pea roots inoculated with biosensors in wild-type Rlv3841 and Rlv3841 *nodC128*::Tn*5* mutant background. Only wild-type Rlv3841 strains are able to form nodules. Biosensors detect: polyols, erythritol (A, E and I) (scale: 100-1,000) and mannitol (B, F and J) (scale: 50-700), the organic acids, formate (C, G and K) (scale: 100-2,000) and salicylic acid (D, H and L) (scale: 100-2,000). A-D, Images representative of biosensors in Rlv3841 background. E-H, Comparison of mean luminescence (pxl mm^{-2}) from pea roots inoculated with biosensors in wild-type Rlv3841 background (dark gray) and Rlv3841 *nodC128*::Tn*5* background (light gray). Standard errors are shown by bars. I-L, Images representative of biosensors in Rlv3841 *nodC128*::Tn*5* mutant background.

Supplemental Figure S7. Comparison of mean luminescence (cps mm^{-2}) of pea nodules from 15 to 22 dpi, with biosensors in wild-type Rlv3841 background. Biosensors are specific for: xylose (A), fructose (B), phenylalanine (C) and hesperetin (D). Standard errors are shown by bars.

Supplemental Figure S8. *In vivo* spatial and temporal mapping images of pea roots with biosensors detecting: sucrose (A) (scale: 200-65,535 cps), *myo*-inositol (B) (scale: 50-2,000 cps), malonate (C) (scale: 50-2,000 cps) and phenylalanine (D) (scale: 150-15,000 cps). Images were acquired at 4, 8, 11, 15, 18 and 22 dpi. These images are representative of those from biosensors in Rlv3841 *nodC128*::Tn*5* background and are unable to nodulate peas.

Supplemental Figure S9. *In vivo* spatial and temporal mapping images of pea roots with biosensors detecting: sugars, xylose (A) (scale: 400-12,000 cps) and fructose (B) (scale: 300-12,000 cps), organic acids, C4-dicarboxylates (C) (scale: 400-65,535 cps) and tartrate (D) (scale: 200-15,000), amino acid, GABA (E) (scale: 500-10,000 cps) and flavonoid, hesperetin (F) (scale: 250-13,000 cps). Images were acquired at 4, 8, 11, 15, 18 and 22 dpi. These images are representative of those from biosensors in Rlv3841 *nodC128*::Tn*5* background and are unable to nodulate peas.

Supplemental Figure S10. Comparison of mean luminescence (cps mm^{-2}) from pea roots inoculated with biosensors in wild-type Rlv3841 background (dark gray) and Rlv3841 *nifH*::ΩSp mutant background (white). Values for *nifH*::ΩSp mutant are adjusted for the lower level of constitutive Lux expression in this background (Fig. 4) to show equivalent expression in a wild-type background. Only wild-type Rlv3841 strains are able to form nitrogen-fixing nodules. Biosensors detect: sucrose (A), *myo*-inositol (B), C4-dicarboxylates (C), and GABA (D). Standard errors are shown by bars and stars indicate significant differences between a biosensor in wild-type Rlv3841 and Rlv3841 *nifH*::ΩSp mutant background (t-test, * = $p < 0.05$; ** = $p < 0.01$).

Supplemental Figure S11. Investigation of the role of malonate during root attachment. A, Whole root attachment assay showing the number of bacteria attached after 1 h incubation for wild-type Rlv3841[pIJ11282], Rlv3841 *matC*::pK19 [pIJ11282] and Rlv3841 *matA*::pK19[pIJ11282], mutated in malonate transport and catabolism respectively. Plasmid pIJ11282 has constitutively expressed *lux* genes (Frederix et al., 2014). Standard errors are shown by bars. Different letters are used to indicate significant difference (ANOVA with post hoc HSD Tukey test, $p < 0.05$) between groups. B, Competition test on pea plants at 7 dpi. Histograms represent luminescence/area of constitutive reporter pIJ11282. Strains Rlv3841[pIJ11282] or Rlv3841 *matC*::pK19 [pIJ11282] were inoculated in ratio 1:1 with Rlv3841 or Rlv3841 *matC*::pK19. Standard errors are shown by bars.

Supplemental Table S1. Strains and plasmids used in this work. St (streptomycin), Neo (neomycin), Tc (tetracycline) and Sp (spectinomycin).

Supplemental Table S2. Conditions used to test specificity the bioreporter library.

Supplemental Table S3. Metabolomic data from root exudates of *P. sativum.*

Supplemental Table S4. ANOVAs with post hoc Tukey test ($p < 0.05$) on total luminescence for bioreporters in Rlv3841 inoculated onto pea plants (Fig. 2 and 3).

Supplemental Table S5. ANOVAs with post hoc Tukey test ($p < 0.05$) on total luminescence for bioreporters in Rlv3841 *nodC128*::Tn*5* inoculated onto pea plants (Fig. 2 and 3).

Supplemental Table S6. ANOVAs with post hoc Tukey test ($p < 0.05$) on nodules luminescence for bioreporters in Rlv3841 inoculated onto pea plants (Fig. 4).

Supplemental Table S7. ANOVAs with post hoc Tukey test ($p < 0.05$) on nodules luminescence for bioreporters in Rlv3841 *nifH*::ΩSp inoculated onto pea plants (Fig. 4).

Supplemental Table S8. ANOVAs with post hoc Tukey test ($p < 0.05$) on total luminescence for bioreporters in Rlv3841 inoculated onto vetch plants (Fig. 5).

Supplemental Table S9. Primers used in this work.

Supplemental Table S10. Relative expression in microarray experiments under seventy-three different conditions of the *R. leguminosarum* genes whose promoters were used for construction of biosensors.

1085 **Table I.** *Characterization of biosensors from R. leguminosarum*
1086

Biosensor	Inducer(s)	Fold-induction	Sensitivity (mM)	Specific luminescence (RLU/OD_{600})	Gene	Name	Function of protein encoded by gene
Sugars and polyols							
Xylose	Xylose	7.20 (±0.34)	1	1.10×10^7	RL2720[b]	*rbsC*	Transport, permease of ABC, CUT2
	Lyxose	6.99 (±0.37)		1.12×10^7			
Fructose	Fructose	16.13 (±1.07)	0.01	2.84×10^7	RL0489[c]	*frcB*	Transport, SBP of ABC, CUT2
	Lactulose	11.10 (±0.87)		1.97×10^7			
	Mannitol	8.94 (±0.26)		1.51×10^7			
	Mannose	8.41 (±0.46)		1.47×10^7			
	Sorbitol	8.94 (±0.58)		1.61×10^7			
	Sucrose	7.00 (±0.21)		1.18×10^7			
Sucrose	Sucrose	36.35 (±1.77)	0.1	2.94×10^7	pRL120556[c]		Transport, SBP of ABC, CUT1
	Raffinose	34.19 (±4.43)		2.93×10^7			
Erythritol	Erythritol	4.72 (±0.50)	1	2.47×10^5	pRL90085[b]		Transport, SBP of ABC, CUT2
Mannitol	Mannitol	1.71×10^6 ($\pm 1.50 \times 10^6$)	0.001	5.51×10^{12}	RL4218[b]		Transport, solute binding protein (SBP) of ABC, CUT1
	Sorbitol[a]	28.52 (±3.53)		3.45×10^7			
	Adonitol[a]	13.01 (±2.39)		1.45×10^7			
***myo*-Inositol**	*myo*-Inositol	216.84 (±13.80)	0.1	4.00×10^7	RL4655[b,c]	*intA*	Transport, SBP of ABC, CUT2
Organic acids							
Formate	Formate	27.20 (±2.13)	10	2.02×10^6	RL4393[b]	*fdsG*	Metabolism, formate dehydrogenase
Malonate	Malonate	540.48 (±155.87)	10	5.69×10^6	RL0990[b]	*matA*	Metabolism
C4-dicarboxylates	Succinate	87.83 (±3.46)	0.1	2.28×10^7	RL3424[b]	*dctA*	Transport, dicarboxylate transporter
	Malate	57.19 (±9.18)	0.01	2.86×10^7			

	Aspartate	33.18 (±3.02)	10	1.28×10^7			
Tartrate	Tartrate	188.68 (±10.51)	0.1	2.32×10^7	RL0996[b]		Transport, permease of MFS uptake system
Salicylic acid	Salicylic acid	1024.87 (±161.97)	1	1.78×10^7	RL1329	*salA*	Transport, MFS efflux system
Amino acids							
Phenylalanine	Phenylalanine	52.10 (±8.43)	0.01	4.08×10^7	RL1860[b]	*phhA*	Metabolism, phenylalanine-4-hydroxylase
GABA	GABA	3.56 (±1.28)	0.5	5.34×10^4	RL0102[d]	*gabT*	Metabolism, 4-aminobutyrate aminotransferase
Flavonoids							
Hesperetin	Hesperetin	256.44 (±68.68)	0.001	1.63×10^7	pRL100185[b,c]	*nodABC*	Metabolism, Nod factor synthesis

Abbreviations used: RLU (relative luminescence units), ABC (ATP binding cassette transporter); CUT1, CUT2 (carbohydrate uptake transporter-1 and -2); SBP (substrate binding protein); MFS (major facilitator superfamily). Inducer(s) are solute(s) that give the highest fold-induction and specific luminescence. Biosensor induction by a solute is described as specific if the specific luminescence is ≥10-fold that observed from the other solutes tested. The biosensors for erythritol, formate, and GABA have a relatively high expression with a variety of non-related solutes (background) and they are described as being specific for these solutes, respectively, with specific luminescence ≥4-fold values obtained with other solutes. More than one compound is considered inducing when the fold-induction is > 40% of the maximum fold-induction for a biosensor. Fold-induction is the ratio of RLU/OD_{600} when grown in the presence of solute (Supplemental Table S2 gives solute concentration), to RLU/OD_{600} when grown in absence of solute. Sensitivity is the minimum concentration of substrate spotted onto bacteria growing in agar to give a luminescent signal visible with a NightOWL camera after 4 h incubation. [a] Fold-induction is <40% that of the best inducer and therefore not considered to be specific induction. [b] indicates genes induced >3-fold, $p \leq 0.05$ in the pea rhizosphere (Ramachandran et al. 2011). [c] indicates genes induced >3-fold, $p \leq 0.05$ by pea exudate (Ramachandran et al. 2011). [d] indicates genes induced >3-fold, $p \leq 0.05$ in the alfalfa rhizosphere (Ramachandran et al. 2011).

Table II. *Results from microarrays comparing the effect of pea root exudate and the pea rhizosphere on expression of genes used to develop biosensors*

Biosensor	Gene	Fold-expression with added 23 d-old pea root exudate [a,b]	Fold-expression in 21 d-old pea rhizosphere [b,c]
Sugars and polyols			
Xylose	RL2720	1.21†	4.00
Fructose	RL0489	18.52	1.65
Sucrose	pRL120556	3.31	1.03†
Erythritol	pRL90085	1.34†	5.74
Mannitol	RL4218	4.30†	3.18
***myo*-Inositol**	RL4655	26.94	2.71
Organic acids			
Formate[d]	RL4393	0.88†	7.52
Malonate	RL0992	1.48†	1.31†
C4-dicarboxylates	RL3424	0.67†	23.00
Tartrate	RL0996	3.34†	5.70
Salicylic acid[d]	RL1329	1.18†	2.27
Amino acids			
Phenylalanine	RL1860	0.86†	46.28
GABA	RL0102	2.90	1.14†
Flavonoids			
Hesperetin[d]	pRL100185	49.15	2.09

[a] Microarrays performed in triplicate on free-living Rlv3841cells grown with and without the addition of pea root exudate (part of the sample used for metabolomic analysis). [b] $p \leq 0.05$, unless marked † when $p > 0.05$; fold-expression >1 are an increase in expression under the condition tested. [c] Microarrays performed in triplicate on Rlv3841 extracted from rhizosphere compared with free-living cells grown in glucose/ammonia (Ramachandran et al., 2011). [d] Compound not found in metabolomic analysis of pea root exudate.

Table III. *Summary of compounds detected by biosensors in the pea rhizosphere and within nodules of Rlv3841*

Compound	Rhizosphere 4-11 dpi	Location on roots	Nodules 11-22 dpi	Nodule age at which detection peaks (dpi)
Sugars and polyols				
Xylose	Yes	Primary and lateral root tips	Yes	15-18
Fructose	Yes	Primary and lateral root tips	Yes	15-22
Sucrose	No		Yes	15-18
Erythritol[a]	No		No	
Mannitol[a]	No		No	
myo-Inositol	Yes	Primary root and lateral root tips	Yes	15-18
Organic acids				
Formate[a,b]	No		No	
Malonate	Yes	Uppermost portion of primary root and lateral roots, just before root tips	Low	15
C4-dicarboxylates	Yes	No clear pattern	Yes	15-18
Tartrate	Yes	Uppermost portion of primary root only	Low	15
Salicylic acid[a,b]	No		No	
Amino acids				
Phenylalanine	Yes	Root elongation zone of lateral roots	Yes	15
GABA	No		Yes	15-18
Flavonoids				
Hesperetin[b]	Yes	Lateral roots	Yes	15

[a] Luminescence from biosensor detecting this compound was very low throughout the time course examining the pea rhizosphere.[b] Compound not listed as present in metabolomics analysis of pea exudate. dpi, days post-inoculation.

Table IV. *Summary of compounds detected by biosensors in the vetch rhizosphere and within nodules of Rlv3841*

Compound	Rhizosphere 4 dpi	Nodules 8-22 dpi	Nodule age at which detection peaks (dpi)[a]
Sugars and polyols			
Xylose	Yes	Yes	22
Fructose	Yes	Yes	(8) 11 (14-22)
Sucrose	No	Yes	(8) 11 (14-22)
Erythritol[b]	No	No	
Mannitol[b]	No	No	
myo-Inositol	Yes	Yes	22
Organic acids			
Formate[b]	No	No	
Malonate	Yes	No	
C4-dicarboxylates	Yes	Yes	(8-11) 14 (18-22)
Tartrate[b]	No	No	
Salicylic acid[b]	No	No	
Amino acids			
Phenylalanine	No	Yes	(18) 22
GABA	No	Yes	8 (11-14)
Flavonoids			
Hesperetin	Yes	No	

[a] Brackets indicate when there is less than the maximum detected. [b] Luminescence from biosensor detecting this compound was very low throughout the time course examining the vetch rhizosphere. dpi, days post-inoculation.

Parsed Citations

Badri DV, Weir TL, van der Lelie D, Vivanco JM (2009) Rhizosphere chemical dialogues: plant-microbe interactions. Curr Opin Biotechnol 20: 642-650
Pubmed: Author and Title
CrossRef: Author and Title
Google Scholar: Author Only Title Only Author and Title

Baetz U, Martinoia E (2014) Root exudates: the hidden part of plant defense. Trends Plant Sci 19: 90-98
Pubmed: Author and Title
CrossRef: Author and Title
Google Scholar: Author Only Title Only Author and Title

Bais HP, Weir TL, Perry LG, Gilroy S, Vivanco JM (2006) The role of root exudates in rhizosphere interactions with plants and other organisms. Annu Rev Plant Biol 57: 233-266
Pubmed: Author and Title
CrossRef: Author and Title
Google Scholar: Author Only Title Only Author and Title

Beringer JE (1974) R factor transfer in Rhizobium leguminosarum. J Gen Microbiol 84: 188-198
Pubmed: Author and Title
CrossRef: Author and Title
Google Scholar: Author Only Title Only Author and Title

Berrabah F, Ratet P, Gourion B (2015) Multiple steps control immunity during the intracellular accommodation of rhizobia. J Exp Bot 66: 1977-1985
Pubmed: Author and Title
CrossRef: Author and Title
Google Scholar: Author Only Title Only Author and Title

Biedrzycki ML, Bais HP (2009) Root secretions: from genes and molecules to microbial associations. J Exp Bot 60: 1533-1534
Pubmed: Author and Title
CrossRef: Author and Title
Google Scholar: Author Only Title Only Author and Title

Chabot R, Antoun H, Kloepper JW, Beauchamp CJ (1996) Root colonization of maize and lettuce by bioluminescent Rhizobium leguminosarum biovar phaseoli. Appl Environ Microbiol 62: 2767-2772
Pubmed: Author and Title
CrossRef: Author and Title
Google Scholar: Author Only Title Only Author and Title

Close D, Xu T, Smartt A, Rogers A, Crossley R, Price S, Ripp S, Sayler G (2012) The evolution of the bacterial luciferase gene cassette (lux) as a real-time bioreporter. Sensors (Basel) 12: 732-752
Pubmed: Author and Title
CrossRef: Author and Title
Google Scholar: Author Only Title Only Author and Title

Darwent MJ, Paterson E, McDonald AJ, Tomos AD (2003) Biosensor reporting of root exudation from Hordeum vulgare in relation to shoot nitrate concentration. J Exp Bot 54: 325-334
Pubmed: Author and Title
CrossRef: Author and Title
Google Scholar: Author Only Title Only Author and Title

Downie JA, Knight CD, Johnston AWB, Rossen L (1985) Identification of genes and gene products involved in the nodulation of peas by Rhizobium leguminosarum. Molecular and General Genetics 198: 255-262
Pubmed: Author and Title
CrossRef: Author and Title
Google Scholar: Author Only Title Only Author and Title

Evans AM, DeHaven CD, Barrett T, Mitchell M, Milgram E (2009) Integrated, nontargeted ultrahigh performance liquid chromatography/electrospray ionization tandem mass spectrometry platform for the identification and relative quantification of the small-molecule complement of biological systems. Anal Chem 81: 6656-6667
Pubmed: Author and Title
CrossRef: Author and Title
Google Scholar: Author Only Title Only Author and Title

Figurski DH, Helinski DR (1979) Replication of an origin-containing derivative of plasmid RK2 dependent on a plasmid function provided in trans. Proc Natl Acad Sci U S A 76: 1648-1652
Pubmed: Author and Title
CrossRef: Author and Title
Google Scholar: Author Only Title Only Author and Title

Frederix M, Edwards A, Swiderska A, Stanger A, Karunakaran R, Williams A, Abbruscato P, Sanchez-Contreras M, Poole PS, Downie JA (2014) Mutation of praR in Rhizobium leguminosarum enhances root biofilms, improving nodulation competitiveness by increased expression of attachment proteins. Mol Microbiol 93: 464-478
Pubmed: Author and Title
CrossRef: Author and Title
Google Scholar: Author Only Title Only Author and Title

Galardini M, Brilli M, Spini G, Rossi M, Roncaglia B, Bani A, Chiancianesi M, Moretto M, Engelen K, Bacci G, Pini F, Biondi EG,

Bazzicalupo M, Mengoni A (2015) Evolution of intra-specific regulatory networks in a multipartite bacterial genome. PLoS Comput Biol 11: e1004478
Pubmed: Author and Title
CrossRef: Author and Title
Google Scholar: Author Only Title Only Author and Title

Huang X-F, Chaparro JM, Reardon KF, Zhang R, Shen Q, Vivanco JM (2014) Rhizosphere interactions: root exudates, microbes, and microbial communities. Botany 92: 267-275
Pubmed: Author and Title
CrossRef: Author and Title
Google Scholar: Author Only Title Only Author and Title

Kaiser C, Kilburn MR, Clode PL, Fuchslueger L, Koranda M, Cliff JB, Solaiman ZM, Murphy DV (2015) Exploring the transfer of recent plant photosynthates to soil microbes: mycorrhizal pathway vs direct root exudation. New Phytol 205: 1537-1551
Pubmed: Author and Title
CrossRef: Author and Title
Google Scholar: Author Only Title Only Author and Title

Karunakaran R, East AK, Poole PS (2013) Malonate catabolism does not drive N(2) fixation in legume nodules. Applied and Environmental Microbiology 79: 4496-4498
Pubmed: Author and Title
CrossRef: Author and Title
Google Scholar: Author Only Title Only Author and Title

Karunakaran R, Ramachandran VK, Seaman JC, East AK, Mouhsine B, Mauchline TH, Prell J, Skeffington A, Poole PS (2009) Transcriptomic analysis of Rhizobium leguminosarum biovar viciae in symbiosis with host plants Pisum sativum and Vicia cracca. J Bacteriol 191: 4002-4014
Pubmed: Author and Title
CrossRef: Author and Title
Google Scholar: Author Only Title Only Author and Title

Kiers ET, Rousseau RA, West SA, Denison RF (2003) Host sanctions and the legume-rhizobium mutualism. Nature 425: 78-81
Pubmed: Author and Title
CrossRef: Author and Title
Google Scholar: Author Only Title Only Author and Title

Lawton KA, Berger A, Mitchell M, Milgram KE, Evans AM, Guo L, Hanson RW, Kalhan SC, Ryals JA, Milburn MV (2008) Analysis of the adult human plasma metabolome. Pharmacogenomics 9: 383-397
Pubmed: Author and Title
CrossRef: Author and Title
Google Scholar: Author Only Title Only Author and Title

Maj D, Wielbo J, Marek-Kozaczuk M, Skorupska A (2010) Response to flavonoids as a factor influencing competitiveness and symbiotic activity of Rhizobium leguminosarum. Microbiol Res 165: 50-60
Pubmed: Author and Title
CrossRef: Author and Title
Google Scholar: Author Only Title Only Author and Title

Mauchline TH, Fowler JE, East AK, Sartor AL, Zaheer R, Hosie AH, Poole PS, Finan TM (2006) Mapping the Sinorhizobium meliloti 1021 solute-binding protein-dependent transportome. Proc Natl Acad Sci U S A 103: 17933-17938
Pubmed: Author and Title
CrossRef: Author and Title
Google Scholar: Author Only Title Only Author and Title

Maxwell CA, Hartwig UA, Joseph CM, Phillips DA (1989) A Chalcone and Two Related Flavonoids Released from Alfalfa Roots Induce nod Genes of Rhizobium meliloti. Plant Physiol 91: 842-847
Pubmed: Author and Title
CrossRef: Author and Title
Google Scholar: Author Only Title Only Author and Title

Mooney SJ, Pridmore TP, Helliwell J, Bennett MJ (2011) Developing X-ray Computed Tomography to non-invasively image 3-D root systems architecture in soil. Plant and Soil 352: 1-22
Pubmed: Author and Title
CrossRef: Author and Title
Google Scholar: Author Only Title Only Author and Title

Oburger E, Schmidt H (2016) New Methods To Unravel Rhizosphere Processes. Trends Plant Sci 21: 243-255
Pubmed: Author and Title
CrossRef: Author and Title
Google Scholar: Author Only Title Only Author and Title

Oldroyd GE, Murray JD, Poole PS, Downie JA (2011) The rules of engagement in the legume-rhizobial symbiosis. Annu Rev Genet 45: 119-144
Pubmed: Author and Title
CrossRef: Author and Title
Google Scholar: Author Only Title Only Author and Title

Philippot L, Raaijmakers JM, Lemanceau P, van der Putten WH (2013) Going back to the roots: the microbial ecology of the rhizosphere. Nat Rev Microbiol 11: 789-799
Pubmed: Author and Title

CrossRef: Author and Title
Google Scholar: Author Only Title Only Author and Title

Pini F, Galardini M, Bazzicalupo M, Mengoni A (2011) Plant-bacteria association and symbiosis: are there common genomic traits in alphaproteobacteria? Genes (Basel) 2: 1017-1032
Pubmed: Author and Title
CrossRef: Author and Title
Google Scholar: Author Only Title Only Author and Title

Poole P, Allaway D (2000) Carbon and nitrogen metabolism in Rhizobium. Adv Microb Physiol 43: 117-163
Pubmed: Author and Title
CrossRef: Author and Title
Google Scholar: Author Only Title Only Author and Title

Poole PS, Schofield NA, Reid CJ, Drew EM, Walshaw DL (1994) Identification of chromosomal genes located downstream of dctD that affect the requirement for calcium and the lipopolysaccharide layer of Rhizobium leguminosarum. Microbiology 140 (Pt 10): 2797-2809
Pubmed: Author and Title
CrossRef: Author and Title
Google Scholar: Author Only Title Only Author and Title

Ramachandran VK, East AK, Karunakaran R, Downie JA, Poole PS (2011) Adaptation of Rhizobium leguminosarum to pea, alfalfa and sugar beet rhizospheres investigated by comparative transcriptomics. Genome Biol 12: R106
Pubmed: Author and Title
CrossRef: Author and Title
Google Scholar: Author Only Title Only Author and Title

Sambrook J, Fritsch EF, Maniatis T (1989) Molecular cloning : a laboratory manual, Ed 2nd. Cold Spring Harbor Laboratory, Cold Spring Harbor, N.Y.
Pubmed: Author and Title
CrossRef: Author and Title
Google Scholar: Author Only Title Only Author and Title

Schloter M, Wiehe W, Assmus B, Steindl H, Becke H, Hoflich G, Hartmann A (1997) Root colonization of different plants by plant-growth-promoting Rhizobium leguminosarum bv. trifolii R39 studied with monospecific polyclonal antisera. Appl Environ Microbiol 63: 2038-2046
Pubmed: Author and Title
CrossRef: Author and Title
Google Scholar: Author Only Title Only Author and Title

Somasegaran P, Hoben HJ (1994) Handbook for Rhizobia: Methods in Legume-Rhizobium Technology. Springer-Verlag, New York
Pubmed: Author and Title
CrossRef: Author and Title
Google Scholar: Author Only Title Only Author and Title

Sørensen J, Haubjerg Nicolaisen M, Ron E, Simonet P (2009) Molecular tools in rhizosphere microbiology—from single-cell to whole-community analysis. Plant and Soil 321: 483-512
Pubmed: Author and Title
CrossRef: Author and Title
Google Scholar: Author Only Title Only Author and Title

Tecon R, van der Meer JR (2006) Information from single-cell bacterial biosensors: what is it good for? Curr Opin Biotechnol 17: 4-10
Pubmed: Author and Title
CrossRef: Author and Title
Google Scholar: Author Only Title Only Author and Title

Terpolilli JJ, Hood GA, Poole PS (2012) What determines the efficiency of N2-fixing Rhizobium-legume symbioses? Adv Microb Physiol 60: 325-389
Pubmed: Author and Title
CrossRef: Author and Title
Google Scholar: Author Only Title Only Author and Title

Terpolilli JJ, Masakapalli SK, Karunakaran R, Webb IU, Green R, Watmough NJ, Kruger NJ, Ratcliffe RG, Poole PS (2016) Lipogenesis and Redox Balance in Nitrogen-Fixing Pea Bacteroids. J Bacteriol 198: 2864-2875
Pubmed: Author and Title
CrossRef: Author and Title
Google Scholar: Author Only Title Only Author and Title

Tett AJ, Karunakaran R, Poole PS (2014) Characterisation of SalRAB a salicylic acid inducible positively regulated efflux system of Rhizobium leguminosarum bv viciae 3841. PLoS One 9: e103647
Pubmed: Author and Title
CrossRef: Author and Title
Google Scholar: Author Only Title Only Author and Title

Tomek J, Novak O, Syka J (2013) Two-Photon Processor and SeNeCA: a freely available software package to process data from two-photon calcium imaging at speeds down to several milliseconds per frame. J Neurophysiol 110: 243-256
Pubmed: Author and Title
CrossRef: Author and Title
Google Scholar: Author Only Title Only Author and Title

Turner TR, James EK, Poole PS (2013a) The plant microbiome. Genome Biol 14: 209
Pubmed: Author and Title
CrossRef: Author and Title
Google Scholar: Author Only Title Only Author and Title

Turner TR, Ramakrishnan K, Walshaw J, Heavens D, Alston M, Swarbreck D, Osbourn A, Grant A, Poole PS (2013b) Comparative metatranscriptomics reveals kingdom level changes in the rhizosphere microbiome of plants. ISME J 7: 2248-2258
Pubmed: Author and Title
CrossRef: Author and Title
Google Scholar: Author Only Title Only Author and Title

Udvardi M, Poole PS (2013) Transport and metabolism in legume-rhizobia symbioses. Annu Rev Plant Biol 64: 781-805
Pubmed: Author and Title
CrossRef: Author and Title
Google Scholar: Author Only Title Only Author and Title

Yagi K (2007) Applications of whole-cell bacterial sensors in biotechnology and environmental science. Appl Microbiol Biotechnol 73: 1251-1258
Pubmed: Author and Title
CrossRef: Author and Title
Google Scholar: Author Only Title Only Author and Title

Ye H, Gemperline E, Venkateshwaran M, Chen R, Delaux P-M, Howes-Podill M, Ane J-M, Li L (2013) MALDI mass spectrometry-assisted molecular imaging of metabolites during nitrogen fixation in the Medicago truncatula- Sinorhizobium meliloti symbiosis. The Plant Journal 75: 130-145
Pubmed: Author and Title
CrossRef: Author and Title
Google Scholar: Author Only Title Only Author and Title

Yobi A, Wone BWM, Xu W, Alexander DC, Guo L, Ryals JA, Oliver M, Cushman JC (2012) Comparative metabolic profiling between desiccation-sensitive and desiccation-tolerant species of Selaginella reveals insights into the resurrection trait. The Plant Journal 72: 983-99
Pubmed: Author and Title
CrossRef: Author and Title
Google Scholar: Author Only Title Only Author and Title